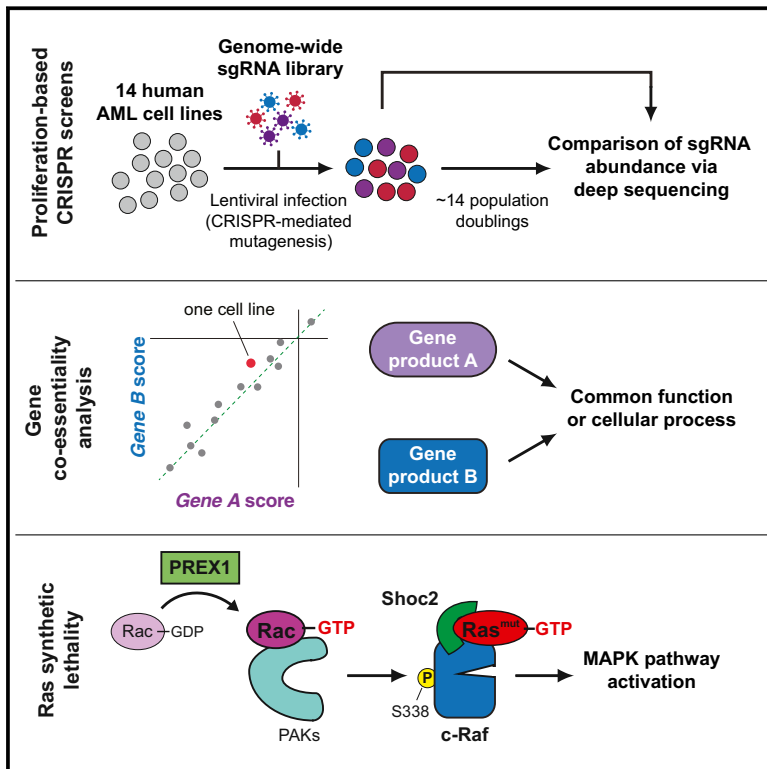# Cell

Gene Essentiality Profiling Reveals Gene Networks and Synthetic Lethal Interactions with Oncogenic Ras

Graphical Abstract

Authors
Tim Wang, Haiyan Yu,
Nicholas W. Hughes, ..., Walter W. Chen,
Eric S. Lander, David M. Sabatini

Correspondence
lander@broadinstitute.org (E.S.L.),
sabatini@wi.mit.edu (D.M.S.)

In Brief

Charting global genetic interaction networks in human cells with CRISPR-based screens uncovers key Ras interactors.

Highlights

- CRISPR-based screens identify essential genes in 14 human AML cell lines

- Analysis of correlated gene essentiality reveals functional gene networks

- Two independent approaches uncover a restricted set of Ras synthetic lethal interactions

- *PREX1* and the Rac pathway are critical regulators of MAPK pathway activation

CellPress

Gene Essentiality Profiling Reveals Gene Networks and Synthetic Lethal Interactions with Oncogenic Ras

Tim Wang,[1,2,3,4,5] Haiyan Yu,[2] Nicholas W. Hughes,[2,3,4,5] Bingxu Liu,[2,3,4,5] Arek Kendirli,[2,6] Klara Klein,[2,6] Walter W. Chen,[1,2,3,4,5] Eric S. Lander,[1,2,7,*] and David M. Sabatini[1,2,3,4,5,8,*]
[1]Department of Biology, Massachusetts Institute of Technology, Cambridge, MA 02139, USA
[2]Broad Institute of MIT and Harvard, Cambridge, MA 02142, USA
[3]Whitehead Institute for Biomedical Research, Cambridge, MA 02142, USA
[4]David H. Koch Institute for Integrative Cancer Research at MIT, Cambridge, MA 02139, USA
[5]Howard Hughes Medical Institute, Department of Biology, Massachusetts Institute of Technology, Cambridge, MA 02139, USA
[6]German Cancer Research Center (DKFZ), 69120 Heidelberg, Germany
[7]Department of Systems Biology, Harvard Medical School, Boston, MA 02115, USA
[8]Lead contact
*Correspondence: lander@broadinstitute.org (E.S.L.), sabatini@wi.mit.edu (D.M.S.)
http://dx.doi.org/10.1016/j.cell.2017.01.013

SUMMARY

The genetic dependencies of human cancers widely vary. Here, we catalog this heterogeneity and use it to identify functional gene interactions and genotype-dependent liabilities in cancer. By using genome-wide CRISPR-based screens, we generate a gene essentiality dataset across 14 human acute myeloid leukemia (AML) cell lines. Sets of genes with correlated patterns of essentiality across the lines reveal new gene relationships, the essential substrates of enzymes, and the molecular functions of uncharacterized proteins. Comparisons of differentially essential genes between Ras-dependent and -independent lines uncover synthetic lethal partners of oncogenic Ras. Screens in both human AML and engineered mouse pro-B cells converge on a surprisingly small number of genes in the Ras processing and MAPK pathways and pinpoint *PREX1* as an AML-specific activator of MAPK signaling. Our findings suggest general strategies for defining mammalian gene networks and synthetic lethal interactions by exploiting the natural genetic and epigenetic diversity of human cancer cells.

INTRODUCTION

Cancer is a heterogeneous disease encompassing hundreds of distinct subtypes that differ in genetic makeup and epigenetic state. Because of this heterogeneity, different cancers rely on different pathways for survival as reflected in striking differences in their responses to anticancer agents (Barretina et al., 2012; Garnett et al., 2012). CRISPR-based screens make it possible to systematically identify the genes required for the survival and proliferation of mammalian cells (Gilbert et al., 2014; Koike-Yusa et al., 2014; Shalem et al., 2014; Wang et al.,

2014). Studies in a small number of human cancer cell lines defined a common set of essential genes that participate in basic cellular processes (Hart et al., 2015; Wang et al., 2015). With a gene essentiality catalog that covers a larger number of cell lines, it should be possible to identify genes required in some cancer cells, but not others, and to use these differential essentialities to (1) define sets of genes that function together and (2) pinpoint the genetic liabilities specific to particular cancer subtypes.

The essentiality pattern of a gene across many cell lines (its "essentiality profile") should help decipher molecular function. Genes that act together (e.g., in a common molecular complex or pathway) will likely have similar profiles so that the function of an uncharacterized gene can be inferred by comparing its profile with those of other genes. As many biological processes impact cell proliferation, this "guilt-by-association" approach should be broadly applicable and may circumvent the need for pathway-specific assays. Analogous studies have been successful in mapping genetic networks in budding yeast using panels of engineered strains with defined lesions in a common genetic background (Costanzo et al., 2016; Hughes et al., 2000). As the spectrum of human cancers captures a comparatively broader range of cell states, analyses of cancer cell lines may allow for an even larger exploration of gene interactions and how they vary across cell types.

A catalog of essential genes across human cancer cell lines should greatly aid efforts to find targets for cancer therapy. While sequencing studies of the cancer genome are providing an increasingly complete description of the genetic alterations that accompany tumorigenesis, functional studies are needed to assess the contribution of candidate oncogenes to cancer cell survival (Boehm and Hahn, 2011; Garraway and Lander, 2013; Lawrence et al., 2014). Furthermore, unbiased surveys of gene essentiality can reveal genes that are not mutated but are nonetheless critical for optimal cancer cell fitness (Cheung et al., 2011; Cowley et al., 2014; Kim et al., 2013; Marcotte et al., 2012; Schlabach et al., 2008; Toledo et al. 2015; Tzelepis et al. 2016). By comparing essentiality profiles across large numbers of genomically characterized cell lines, it should be
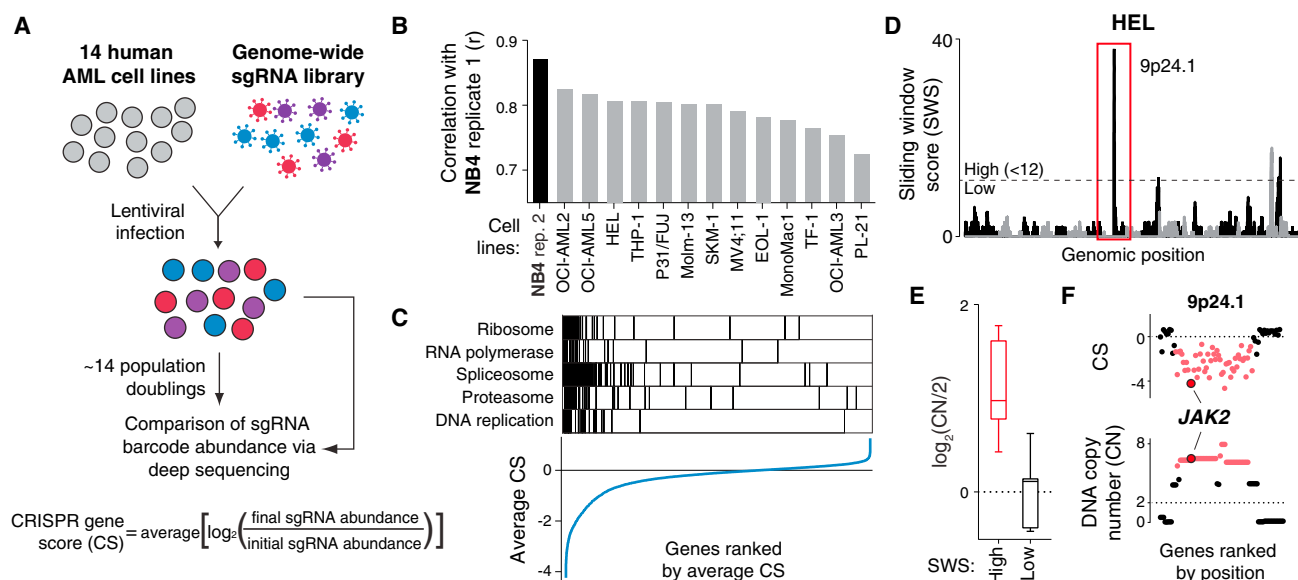
Figure 1. Genome-wide CRISPR Screens for Cell-Essential Genes

(A) Pooled CRISPR-based screening strategy.

(B) CS correlation between cell lines and replicate screens of NB4.

(C) Common cell-essential genes are involved in fundamental biological processes. Gene set enrichment analysis was performed on genes ranked by average CS.

(D–F) SWS analysis. (D) High SWS peaks in HEL that (E) correspond to regions of genomic amplification. (F) Contiguous region of low CS genes reside in amplicon on chromosome 9p24 containing the *JAK2* oncogene.

See also Figure S1 and Tables S1, S2, S3.

possible to identify genes selectively required in cells carrying a specific mutation (Kaelin, 2005). This synthetic lethality paradigm is well illustrated by the interaction between the tumor suppressors *BRCA1/2* and the poly(ADP-ribose) polymerases (PARPs), two gene families involved in parallel DNA repair pathways (Farmer et al., 2005). By exploiting synthetic lethality, it may be possible to develop therapies that treat cancers driven by the loss of a tumor suppressor or an activating mutation in a gene product that is "undruggable." A comprehensive gene essentiality dataset will also address if synthetic lethal interactions tend to occur between genes acting in the same or parallel pathways and how they may be shaped by cellular context.

We perform CRISPR-based genetic screens to generate a comprehensive gene essentiality dataset for a panel of genomically characterized acute myeloid leukemia (AML) cell lines. Analysis of these data and follow-up work reveals the molecular functions of previously unstudied genes and identified new synthetic lethal interactions with mutant Ras, the most common human oncogene. It should be possible to apply the approaches we describe to systematically map functional gene networks in mammalian cells and identify targetable liabilities in human cancers.

RESULTS

Differences in Gene Essentiality Reflect the Distinguishing Characteristics of AML Cell Lines

We performed CRISPR-based screens on a panel of 14 human AML cell lines selected from the Cancer Cell Line Encyclopedia

(Figure 1A; Tables S1, S2, and S3; see the STAR Methods) (Barretina et al., 2012). For each gene in each line, we defined its CRISPR score (CS) as the average $\log_2$ fold-change in the abundance of all single guide (sg)RNAs targeting the gene after 14 population doublings. Replicate screens of NB4 cells were well correlated and the CS from our screens could predict the essentiality of homologs in *S. cerevisiae* (Figures 1B, S1A, and S1B; see the STAR Methods). Consistent with prior work, essential genes highly overlapped between lines and were strongly enriched for roles in fundamental cellular processes (Figure 1C). Additionally, differences in gene essentiality between lines reflected known characteristics, such as cytokine dependence and developmental origin, of each of the lines (Figures S1C–S1F).

We previously demonstrated, and others recently confirmed, that Cas9-mediated cleavage of amplified genomic regions elicits a DNA damage response that causes cell death (Aguirre et al., 2016; Munoz et al., 2016; Wang et al., 2015). Thus, the low CRISPR scores of genes in amplified regions do not necessarily reflect the essentiality of the encoded products and so must be removed from datasets prior to further analyses. We devised a sliding window score (SWS) to identify contiguous stretches of the genome enriched for low scoring genes (see the STAR Methods). The SWS analysis identified several peaks across the genome of HEL cells, all of which corresponded to regions of high-level genomic amplification; the highest peak, residing in an amplicon on 9p24.1, contained *JAK2*, a mutationally activated driver in these cells (Figures 1D–1F) (Quentmeier et al., 2006). High SWS peaks were identified in several of the

other cell lines; the genes within these peaks were also present at high copy number (Figures S1G–S1H). Thus, this simple filtering procedure, which does not rely on DNA copy number information, can be used to identify genes whose low CS are likely artifactual and thus potentially confounding to downstream analyses.

Correlated Gene Essentiality across Cell Lines Reveals Functional Gene Relationships

Genes acting in the same cellular pathway should show similar patterns of essentiality across cell lines, raising the possibility that functional gene networks can be mapped through correlation-based analysis of gene essentiality profiles (Figure 2A). To obtain biologically meaningful gene associations, comparisons must be made between genes showing significant differences in essentiality between lines. Therefore, we chose the most variably essential genes as a query set and searched for co-essential partners for each of these genes. These associations reveal known and novel gene relationships that encompass several types of functional interactions.

Many sets of highly correlated genes encoded physically interacting proteins, including heterodimers involved in transcription (*LDB1* and *LMO2*), PI3-Kγ signaling (*PIK3CG* and *PIK3R5*), amino acid transport (*SLC7A5* and *SLC3A2*), and components of two complexes in the mTOR pathway, mTORC2 (*MAPKAP1*, *MLST8*, and *RICTOR*) and GATOR1 (*NPRL2*, *NPRL3*, and *DEPDC5*) (Figures 2B, 2C, and S2A). This analysis also identified larger protein complexes; nearly all non-redundant components of the Fanconi anemia DNA repair machinery and the GM-CSF receptor pathway clustered tightly together (Figures 2D and S2B). Other sets of genes encoded enzymes catalyzing successive reactions in metabolic pathways (Figure 2E).

Interestingly, we identified a single case of anti-correlation between the p53 tumor suppressor gene (*TP53*) and its negative regulators (Figure 2F). The sgRNAs targeting *TP53* provided a selective advantage (indicated by positive CS) to cells with wild-type, but not mutant, p53. In these same lines, four negative regulators of p53, *TERF1*, a telomere-binding factor; *PPM1D*, a p53-induced phosphatase; *MDM2*, an E3 ubiquitin ligase for p53; and *MDM4*, an inhibitor of p53 transactivation, were selectively required, as their loss presumably induced p53-mediated cell-cycle arrest or apoptosis (Figure S2C).

The correlation analysis also revealed several unexpected gene relationships. For example, the Furin protease cleaves and activates a diverse array of cytokines and growth factor receptors, but in our dataset the essentiality of *FURIN* correlated very highly with that of only one its substrates, the insulin-like growth factor receptor (*IGF1R*), and its adaptor *IRS2* (Bassi et al., 2005) (Figure 2G). This suggests that IGF1R processing may be the only essential function of Furin in cells grown in culture.

We could also examine the opposite problem: identifying enzymes responsible for the maturation of a precursor protein. Activation of the transcription factor Nrf-1 (*NFE2L1*) involves retrotranslocation of Nrf-1 into the cytosol via the ER-associated degradation (ERAD) pathway, deglycosylation by PNGase (*NGLY1*) in the ER, and partial proteolytic digestion by an unidentified protease (Radhakrishnan et al., 2014). Our dataset showed correlated essentiality between *NFE2L1*, *NGLY1*, and the endopeptidase *DDI2* (Figure 2G). These patterns of gene essentiality suggest that DDI2 may be the unknown protease that cleaves Nrf-1. Indeed, very recent work in *C. elegans* indicates that the homolog of DDI2 (C01G5.6) does act on the worm version Nrf-1 (Lehrbach and Ruvkun, 2016).

Our analysis also predicted associations between genes for which no functional relationship has been previously established (Figure 2H). Lastly, several genes of unknown function, such as *C1orf27* and *C17orf89*, had correlated essentialities with genes encoding components of well-characterized pathways, suggesting that they may represent new pathway members. We performed extensive follow-up experiments to determine whether this was indeed the case

C1orf27 Interacts with UFSP2 and Is Required for deUFMylation

The essentiality of *C1orf27* correlated with (1) the essentiality of several genes encoding components of the UFMylation machinery, a ubiquitin-like protein modification system that attaches UFM1 to proteins, and (2) UFM1 expression levels (Figures 3A and 3B) (Komatsu et al., 2004). Interestingly, prior work in *C. elegans* reported that homologs of C1orf27 and its most closely correlated partner, UFSP2, a deUFMylating enzyme, localize to the ER where they directly interact with each other (Chen et al., 2014). We confirmed these findings in human embryonic kidney (HEK)-293T cells stably expressing recombinant human C1orf27 and UFSP2 (Figures 3C and 3D).

C1orf27 is predicted to have a C-terminal transmembrane anchor, which may serve to tether it and UFSP2 to the ER surface (Figure S3A). Consistent with this model, in *C1orf27*-null cells, UFSP2 failed to localize to the ER and instead was dispersed throughout the cytoplasm (Figure 3E). We probed lysates of *C1orf27* null cells, as well as from cells lacking UFM1, UFSP2, and the E1-like UFM1-activating enzyme, UBA5, with an antibody that recognizes free and conjugated UFM1 (Figure 3F). As expected, inactivation of *UFM1* or *UBA5* led to the complete loss of UFMylation activity. In contrast, loss of *C1orf27* or *UFSP2* led to the accumulation of UFM1-conjugated proteins, consistent with a defect in deUFMylation. These results suggest that C1orf27 is an obligate partner of UFSP2 and that this interaction is required for the proper localization and activity of UFSP2.

C17orf89 Is an Assembly Factor for Mitochondrial Complex I

C17orf89, clustered with a large group of mitochondrial genes and in HEK293T cells C17orf89 co-localized with the mitochondrial marker COX IV (Figures 3G and 3H). Mass spectrometric analysis of anti-FLAG-C17orf89 immunoprecipitates revealed an interaction with NDUFAF5, a complex I assembly factor, which we confirmed in co-immunoprecipitation experiments (Figures 3I and S3B). Strikingly, the mitochondrial gene cluster contained several complex I assembly factors, with *NDUFAF5* being the top hit.

Loss of *C17orf89* specifically destabilized complex I, but not other respiratory chain, complexes (Figures 3J and S3C).
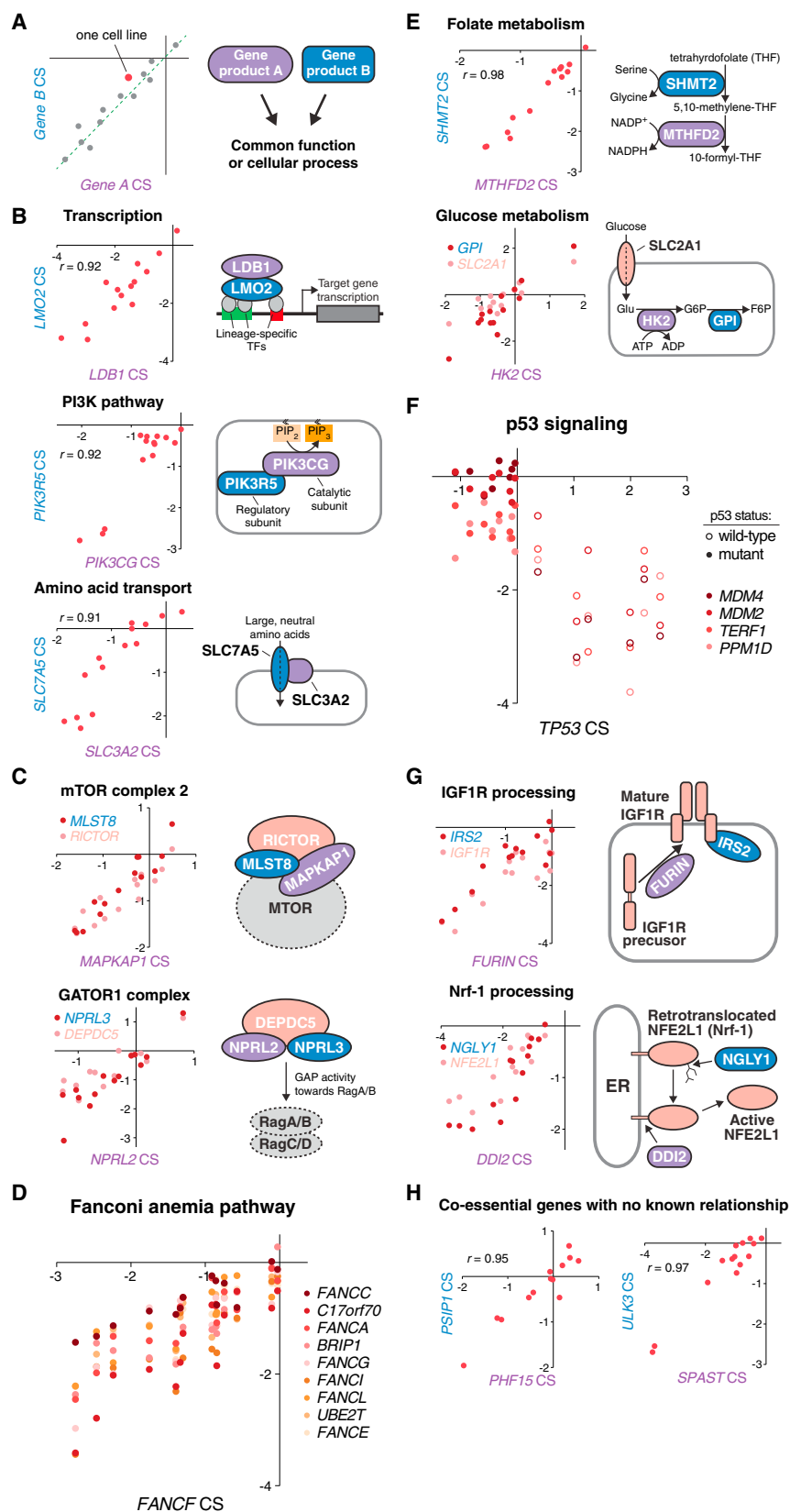
A one cell line

Gene B CS

Gene A CS

Gene product A | Gene product B → **Common function or cellular process**

B Transcription

r = 0.92

LMO2 CS

LDB1 CS

LDB1 / LMO2 → Target gene transcription · Lineage-specific TFs

PI3K pathway

r = 0.92

PIK3R5 CS

PIK3CG CS

PIP₂ → PIP₃ · PIK3CG Catalytic subunit · PIK3R5 Regulatory subunit

Amino acid transport

r = 0.91

SLC7A5 CS

SLC3A2 CS

Large, neutral amino acids · SLC7A5 / SLC3A2

C mTOR complex 2

MLST8 · *RICTOR*

MAPKAP1 CS

RICTOR · MLST8 · MAPKAP1 · MTOR

GATOR1 complex

NPRL3 · *DEPDC5*

NPRL2 CS

DEPDC5 · NPRL2 · NPRL3 · GAP activity towards RagA/B · RagA/B · RagC/D

D Fanconi anemia pathway

FANCC · *C17orf70* · *FANCA* · *BRIP1* · *FANCG* · *FANCI* · *FANCL* · *UBE2T* · *FANCE*

FANCF CS

E Folate metabolism

r = 0.98

SHMT2 CS

MTHFD2 CS

tetrahydrofolate (THF) · Serine → Glycine · SHMT2 · 5,10-methylene-THF · NADP⁺ → NADPH · MTHFD2 · 10-formyl-THF

Glucose metabolism

GPI · *SLC2A1*

HK2 CS

Glucose · SLC2A1 · Glu → G6P → F6P · HK2 · ATP → ADP · GPI

F p53 signaling

TP53 CS

p53 status: wild-type / mutant

MDM4 · *MDM2* · *TERF1* · *PPM1D*

G IGF1R processing

IRS2 · *IGF1R*

FURIN CS

Mature IGF1R · FURIN · IRS2 · IGF1R precursor

Nrf-1 processing

NGLY1 · *NFE2L1*

DDI2 CS

Retrotranslocated NFE2L1 (Nrf-1) · NGLY1 · Active NFE2L1 · DDI2 · ER

H Co-essential genes with no known relationship

r = 0.95

PSIP1 CS

PHF15 CS

r = 0.97

ULK3 CS

SPAST CS

Figure 2. Correlated Gene Essentiality across Cell Lines Uncovers Functional Gene Relationships

(A) Strategy for identifying functionally related sets of genes.

(B–F) Correlated essentiality of genes encoding (B) obligate heterodimers, (C) members of complexes in the mTOR pathway, (D) components of the Fanconi anemia DNA repair pathway, (E) enzymes catalyzing successive metabolic reactions, and (F) negative regulators of p53 that are negatively correlated with *TP53* essentiality. r, Pearson's correlation coefficient.

(G) Top: *FURIN* protease shows correlated essentiality with its substrate *IGF1R* and the *IRS2* signaling adaptor. Bottom: the transcription factor Nrf-1 (encoded by *NFE2L1*) shows correlated essentiality with the *NGLY1* deglycosylase and *DDI2* peptidase.

(H) Correlated essentiality of two sets of genes with no known relationship.

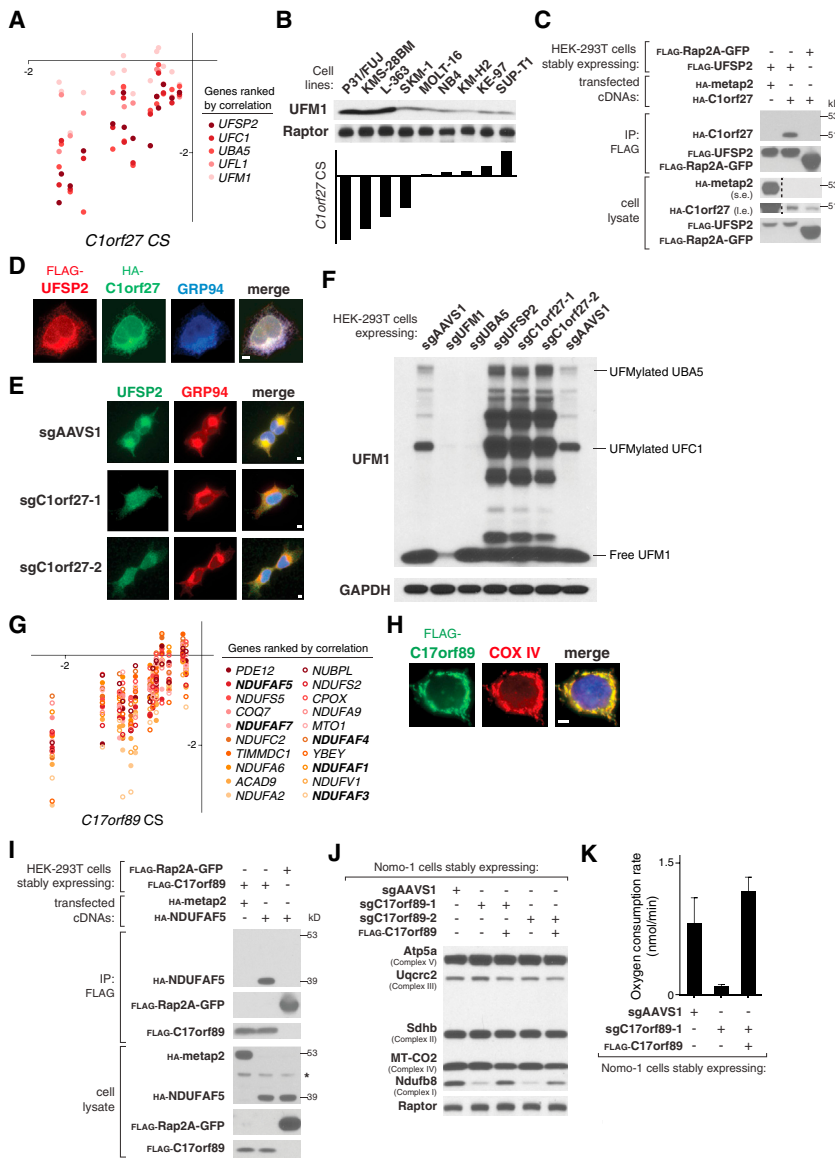See also Figure S2 and Tables S1, S2, S3, S6, S7, and S8.

Figure 3. Correlated Essentiality Analysis Reveals Function of Two Uncharacterized Genes

(A) Correlated essentiality of *C1orf27* with members of the UFMylation pathway.

(B) UFM1 levels correlate with *C1orf27* essentiality.

(C) Recombinant C1orf27 and UFSP2 interact. Rap2A and metap2 served as control bait and prey proteins. s.e., short exposure. l.e., long exposure.

(D) Micrograph of a HEK293T cell stably expressing FLAG-UFSP2 and HA-C1orf27. GRP94 is an ER marker.

(E) C1orf27 is required for the proper localization of UFSP2 in HEK293T cells.

(F) C1orf27 loss results in accumulation of UFMylated proteins. GAPDH served as a loading control.

(G) Correlated essentiality of *C17orf89* with members of the OXPHOS pathway.

(H) Micrograph of a HEK293T cell stably expressing FLAG-C17orf89. COX IV is a mitochondrial marker.

(I) Recombinant C17orf89 and NDUFAF5 interact. *, non-specific band.

(J and K) C17orf89 loss (J) destabilizes mitochondrial complex I and (K) reduces oxygen consumption. Raptor served as a loading control. Error bars represent SD from four replicate wells.

Scale bar, 5 μm.

See also Figure S3 and Tables S1, S2, S3.

does not actually activate the gene, that the oncogene was required for tumor initiation, but not maintenance, or that the cell has acquired a bypass mutation. We compiled a list of candidate oncogenes altered in each of the cytokine-independent AML cell lines based on publically available mutational and cytogenetic data and assessed the contribution of each candidate to cell fitness using our essentiality dataset. Overall, this analysis pinpointed key driver events, including common oncogenic mutations and rare translocations, in 11 of the 12 lines assessed. (As discussed above, HEL cells harbor a recurrent $JAK2^{V617F}$ mutation, but it resides in an amplified region and could not be interrogated in our screens.)

Interestingly, we found that even cell lines harboring the same oncogene showed differences in dependence. Four of the cell lines carry activating mutations in *FLT3*, an established oncogene in AML; while *FLT3* scored as an essential gene in three of these, it did not in PL-21 cells, which were also insensitive to quizartinib, a FLT3 inhibitor (Figures 4A and S4A) (Quentmeier et al., 2003).

Examination of other alterations in PL-21 revealed an uncommon mutation at codon 146 of the *KRAS* proto-oncogene. Residue 146 lies within the nucleotide-binding pocket of Kras and mutation of the corresponding site in Hras enhances its nucleotide exchange activity (Feig and Cooper, 1988). Consistent with Ras pathway activation in PL-21, *KRAS* was essential in this line. Two additional lines had mutations in *KRAS* and three
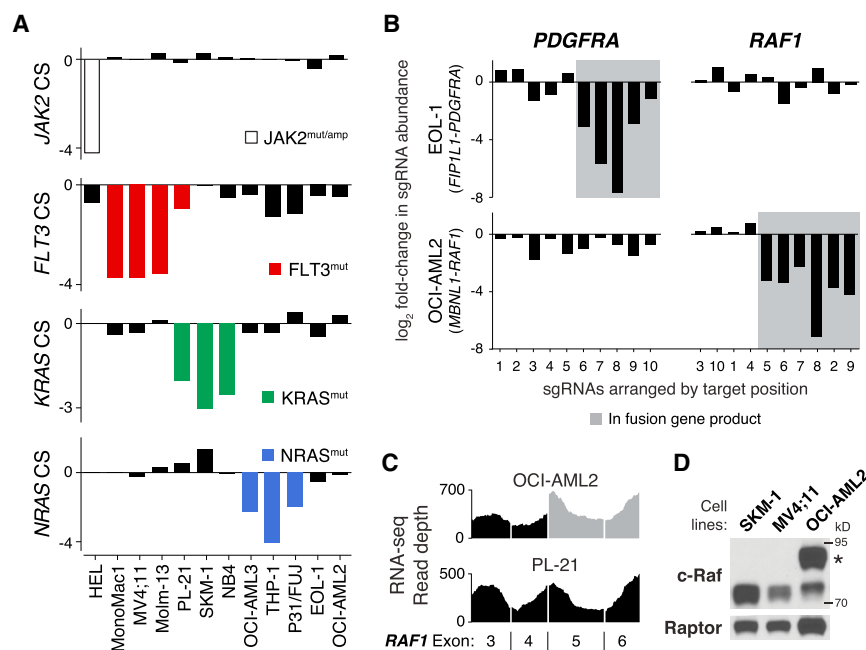
Consistent with a defect in OXPHOS, *C17orf89*-null cells consumed oxygen at a profoundly reduced rate and required the addition of pyruvate to the media to maintain optimal proliferation (Figures 3K and S3D). Importantly, expression of a sgRNA-resistant cDNA rescued these phenotypes. These findings indicate that *C17orf89* encodes a component of the complex I assembly machinery and are in agreement with very recent work which characterized C17orf89 via a proteomics-based approach (Floyd et al., 2016).

Identification of Driver Oncogenes Using an Integrative Genomic Approach

Our gene essentiality catalog can also be used to determine whether a cell line carrying a specific oncogene is actually dependent on the mutated gene. A cell line might not be dependent for several reasons, including that the observed mutation

A

B

C

D

Figure 4. Identification of Driver Oncogenes via an Integrative Genomic Approach

(A) Genomic information and gene essentiality data identify driver oncogenes. *JAK2* is a known driver in HEL cells, but resides in an amplicon and cannot be assessed in our screen.

(B) *PDGFRA* and *RAF1* participate in oncogenic gene fusions. Only gene-fusion-targeting sgRNAs are depleted.

(C) RNA sequencing of OCI-AML2 pinpoints a discontinuity in coverage between exons 4 and 5 of *RAF1*. PL-21 served as a control.

(D) Immunoblotting using an antibody against the C terminus of c-Raf identifies a 90-kDa protein in OCI-AML2. Raptor served as a loading control.

See also Figure S4 and Tables S1, S2, S3.

others in *NRAS*. In all cases, the mutant Ras isoform was selectively essential, whereas wild-type Ras lines did not require any of the individual Ras isoforms.

Our library includes on average ten sgRNAs tiled across the body of each gene allowing for fine-scale analysis of gene fusions. EOL-1 cells harbor a recurrent *FIP1L1-PDGFRA* fusion gene; in these cells, only sgRNAs targeting the fused portion of *PDGFRA* scored, resulting in an atypical, position-dependent pattern of sgRNA depletion (Figure 4B). Translocation partners of the *KMT2A* (MLL) oncogene showed similar patterns in MV4;11 and THP-1 cells (Figure S4B).

We applied this "partial gene essentiality" signature to search for translocated genes in OCI-AML2, which harbors no recurrent oncogenic drivers. Remarkably, our analysis uncovered *RAF1*, which encodes c-Raf, a major Ras effector that regulates the MAPK signaling cascade. Consistent with a previous report, RNA sequencing revealed a chimeric transcript spanning exon 4 of *MBNL1* and exon 5 of *RAF1* that results in the production of a 90-kDa gene product (Figures 4C and 4D) (Klijn et al., 2015). This unique rearrangement removes the N-terminal autoinhibitory domain of c-Raf and likely leads to MAPK pathway activation.

Together, these results illustrate how functional data derived from loss-of-function screens can be integrated with genomic information to identify and validate driver oncogenes.

Two Independent Screening Approaches Reveal Common Synthetic Lethal Interactions with Oncogenic Ras

We also used our data to identify genes that are selectively essential in cell lines carrying particular driver mutations—that is, which have synthetic lethal interactions with the mutated gene. Such genes will typically not be mutated and thus cannot be reliably detected through genome sequencing. They are of significant interest because they may provide drug targets in tumors where

the cancer-causing genes cannot readily be targeted, for example, in those driven by the loss of tumor suppressor genes or by oncogenes that have proven difficult to inhibit directly.

Mutations in the Ras family of GTPases (*KRAS*, *NRAS*, and, less frequently, *HRAS*) are commonly found in many human cancers, including AML, and are associated with poor clinical prognoses (Cox et al., 2014). Ras controls a diverse array of cellular processes through many downstream effectors. As each of these effector pathways is implicated in various aspects of Ras-driven tumorigenesis across different cellular contexts, it has been difficult to dissect the contribution of each pathway to the overall survival and proliferation of cancer cells. Furthermore, it is even less clear if Ras hyper-activation may somehow confer dependence on other, unrelated cellular pathways. Systematic screening approaches have greatly accelerated efforts to find liabilities in Ras-driven cancers (Barbie et al., 2009; Luo et al., 2009a). Here, we employed two independent screening strategies to search for synthetic lethal partners of oncogenic Ras (Figure 5A).

In our initial approach, we looked for genes that showed differential essentiality across the 12 cytokine-independent AML cell lines in our panel. Comparisons between the six Ras-dependent and six Ras-independent revealed five genes that were required only in the context of oncogenic Ras. Two genes (*RCE1* and *ICMT*) are involved in the maturation of Ras. Two additional genes (*RAF1* and *SHOC2*) are involved in MAPK pathway signaling. The final gene, *PREX1*, did not immediately fit in either category and is discussed later in its own section.

Ras is synthesized as an inactive precursor in the cytosol and converted into its mature membrane-associated form through three enzymatic steps: (1) prenylation of the CAAX box by farnesyltransferase (FTase) or geranylgeranyltransferase I (GGTase I), (2) cleavage of the terminal AAX residues by Ras converting enzyme (Rce1), and (3) methylation of the terminal cysteine residue by isoprenylcysteine carboxyl methyltransferase (Icmt). *FNTB*, which encodes a subunit of the FTase, was essential in all cell lines screened, suggesting that FTase acts on a universally essential protein (Figure S5A). *RCE1* and *ICMT*, however,
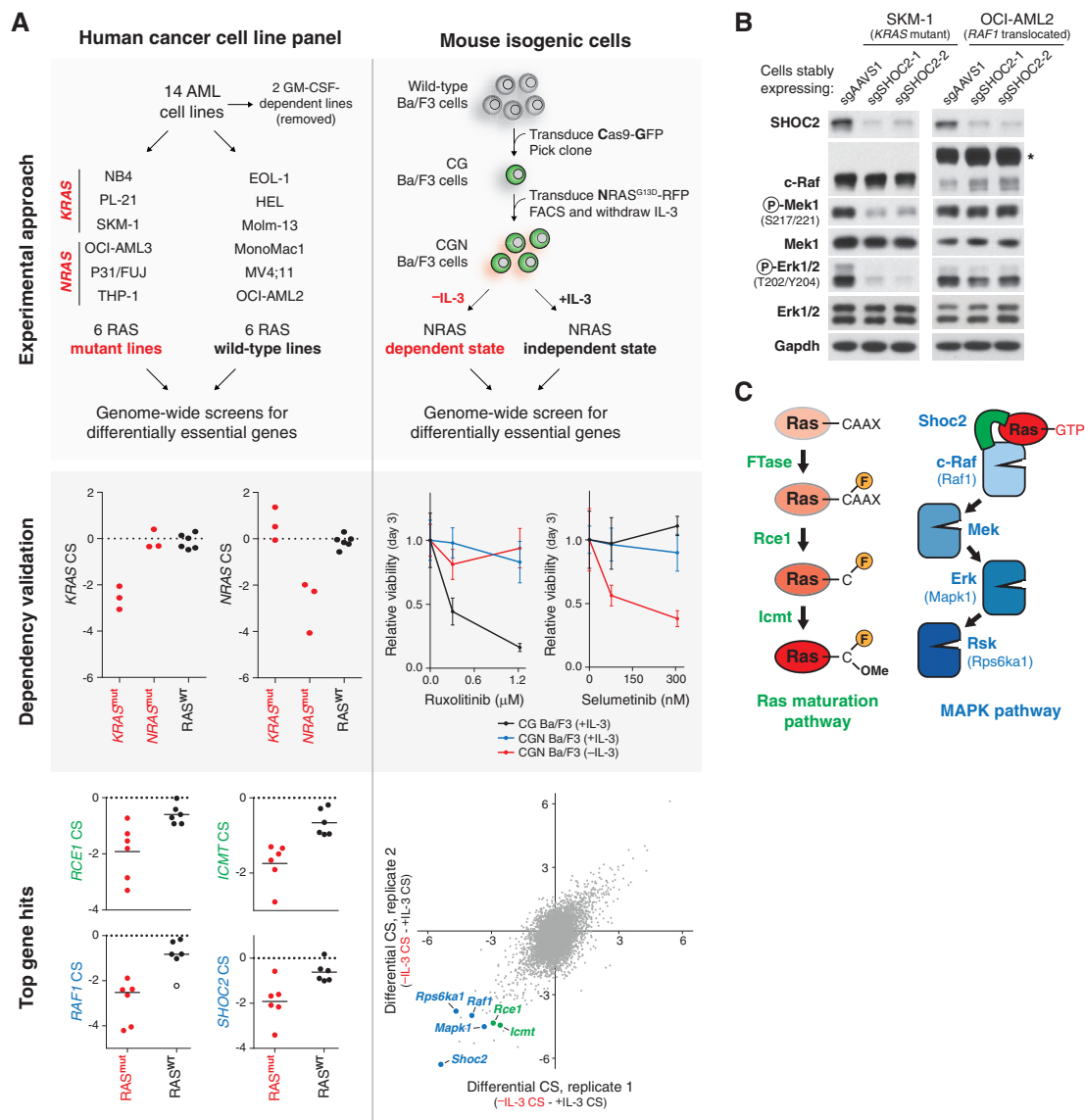
Figure 5. Two Independent Screening Approaches Identify Common Synthetic Lethal Interactions with Oncogenic Ras

(A) Left: differential gene essentiality analysis of 12 cytokine-independent AML cell lines. The three mutant *NRAS* and three mutant *KRAS* cell lines are dependent on the mutated Ras isoform. The open circle in *RAF1* CS plot represents OCI-AML2. Right: Ba/F3 cells were transduced with (**C**)as9-(**G**)FP and (**N**)RAS[G13D] to generate the CGN Ba/F3 line. CGN cells do not rely on JAK/STAT signaling and are conditionally dependent on the Ras pathway as assessed by sensitivity to the JAK and MEK inhibitors, ruxolitinib, and selumetinib. Comparisons between CGN cells cultured in the presence and absence of IL-3 reveals synthetic lethal interactions with oncogenic Ras. Error bars represent SD from six replicate wells.

(B) *SHOC2* loss reduced MAPK pathway activity in *KRAS* mutant SKM-1 cells, but not *RAF1* mutant OCI-AML2 cells. GAPDH served as a loading control.

(C) Ras synthetic lethal gene candidates converged on pathways functioning up- and downstream of Ras.

See also Figure S5 and Tables S1, S2, S3, S4, and S5.

did show differential essentiality, suggesting that they modify a more restricted set of substrates.

Among the Ras effector genes, *RAF1* and *SHOC2* were the only two selectively essential in all Ras-driven lines. *RAF1* encodes c-Raf, a component of the MAPK signaling cascade needed for the initiation of Kras-driven lung cancers (Blasco et al., 2011; Karreth et al., 2011). *SHOC2* encodes a leucine-rich repeat-containing protein that serves as a scaffold for Ras

and c-Raf (Rodriguez-Viciana et al., 2006). Similar to *RAF1* and other Ras pathway members, mutations in *SHOC2* have been identified in patients with Noonan-like syndromes (Cordeddu et al., 2009). Loss of *SHOC2* reduced MAPK pathway activity in Ras mutant SKM-1 cells, but, importantly, not in OCI-AML2 cells in which *RAF1* is constitutively active (Figure 5B).

In parallel, we devised an isogenic screening approach that did not rely on the use of genetically heterogeneous cancer

cell lines. For this purpose, we screened Ba/F3 cells, a murine pro-B cell line, which we engineered to express oncogenic *NRAS* (CGN Ba/F3) (Figure 5A; Tables S4 and S5; see the STAR Methods). CGN Ba/F3 cells cultured in the absence of IL-3 were dependent on Ras/MAPK signaling, but, critically, this dependence was relieved by the addition of IL-3. Therefore, we could identify Ras-associated vulnerabilities by comparing gene essentiality between these two conditions. Notably, because the genetic background of the cells remains fixed in this experiment, differences in essentiality can be directly attributed to Ras dependency (Figure S5C).

Replicate screens revealed a common set of genes selectively required in the absence of IL-3. Remarkably, *Shoc2*, *Raf1*, *Rce1*, and *Icmt* all scored in the top 0.1% of all genes indicating a very high degree of overlap between the two screening approaches. Additional MAPK pathway members (*Braf*, *Rps6ka1*, and *Mapk1*) scored strongly as well. *BRAF* and *MAPK1* did show a differential essentiality in the human AML lines but were dispensable in some of the mutant Ras lines presumably because they expressed redundant members of these kinase families (Figure S5A). We also identified an Nras-specific dependency. After methylation by Icmt, Nras, but not the major Kras isoform (Kras-4B), is palmitoylated. *Golga7*/*GOLGA7*, which encodes a subunit of the palmitoyltransferase, scored in CGN Ba/F3 and two of the three mutant *NRAS* AML lines, but not in any of the mutant *KRAS* or wild-type Ras lines (Swarthout et al., 2005). Other genes, such as the ubiquitin-specific peptidase *Usp32*/*USP32*, scored strongly in CGN Ba/F3 cells and a subset of the mutant Ras AML lines; the biological basis for its selective essentiality remains to be defined.

These two independent screening approaches converged on a restricted set of common dependencies required for the survival and proliferation of Ras-driven cancers. Intriguingly, the majority of these genes are involved in the maturation of Ras itself and the downstream MAPK signaling pathway (Figure 5C).

MAPK Pathway Activation Requires *PREX1* in Mutant Ras AML Cells

The top scoring hit from the human AML screen was *PREX1*, which encodes a Dbl homology-pleckstrin homology domain-containing (DH-PH) guanine nucleotide exchange factor (GEF) for the Rac GTPases (Figure 6A) (Welch et al., 2002). Oddly, while *PREX1* scored strongly in all six mutant Ras AML cell lines, it did not score highly in the CGN Ba/F3 cells. To begin to understand this difference, we designed a focused sgRNA library targeting synthetic lethal candidate and control genes and used it to profile: (1) the 12 cytokine-independent AML lines used in the genome-wide screens; (2) a validation set of five additional mutant Ras AML lines; and (3) 11 mutant and 14 wild-type Ras non-AML cancer cell lines derived from other hematopoietic lineages (Tables S6, S7, and S8). For all 12 of the original AML cell lines, the focused sgRNA library screen results showed the highest correlation with those from genome-wide screens conducted in the same line (Figure S6).

In all cases, the presence of an amplified or mutated allele of *KRAS* or *NRAS* correlated with dependence on *KRAS* and *NRAS*, respectively (Figure 6B). The downstream MAPK

pathway members, *RAF1* and *SHOC2*, were selectively essential in all the Ras-dependent lines as well. The requirement for *PREX1*, however, differed between the cancer types. Whereas *PREX1* was selectively essential in both the original and validation sets of AML cell lines harboring mutant Ras, there was no difference in *PREX1* essentiality between wild-type and mutant Ras lines in the other hematological cancer types.

Given the established biochemical function of *PREX1*, its importance in mutant Ras AML cells likely reflects a requirement for Rac pathway activity. Consistent with this possibility, *Rac1*/*RAC1* scored as essential in the CGN Ba/F3 cells and to some degree in the human AML lines as well (Figures S5A and S5B). To test the importance of the Rac pathway, we asked whether forced activation of Rac1 could bypass the requirement for *PREX1* by screening SKM-1 cells expressing a constitutively active mutant of Rac1 (Rac1^{G12V}) or wild-type Rac1. Consistent with our hypothesis, the dependence on *PREX1* was relieved in Rac1^{G12V}-expressing cells (Figures 6C and 6D).

Previous studies demonstrate that *PREX1* can influence MAPK signaling, suggesting that like the other screen hits, it may also act on the MAPK pathway (Ebi et al., 2013). To examine this possibility, we screened the focused library in SKM-1 cells stably expressing a constitutively active mutant of Mek1 (Mek1^{DD}) or wild-type Mek1. As expected, Mek1 hyper-activation relieved the dependence on the upstream MAPK pathway components, *KRAS*, *RAF1*, and *SHOC2*. Critically, Mek1^{DD} expression also bypassed the requirement for *PREX1*, placing it too upstream of Mek1 (Figures 6E and 6F). The Rac GTPases can induce MAPK signaling by stimulating the p21-activated kinases (PAKs), which, in turn, phosphorylate and activate c-Raf (King et al., 1998). Consistent with this model, Rac1^{G12V}-expressing cells had hyperactive PAK and MAPK signaling and knockdown of *PREX1* inhibited these pathways in wild-type SKM-1 cells (Figures 6G–6I). Together, these data establish *PREX1* as a key input for MAPK pathway activation in Ras-driven AML cells.

Lack of Paralog Expression Explains AML-Specific Dependence on *PREX1*

As *PREX1* is highly expressed in normal myeloid cells, we reasoned that it functions as the major activator of Rac signaling in AML cells, but that perhaps other GEFs promote Rac activity in other cancers. Consistent with this notion, all of the mutant Ras AML lines examined expressed *PREX1*, but only three of the nine non-AML lines did (Figure 7A). Strikingly, *TIAM1*, another DH-PH Rac-GEF, had the opposite expression pattern—it was absent in all the AML lines but robustly expressed in all but one of the non-AML lines. Notably, the one line not expressing *TIAM1*, NU-DHL-1, expressed high levels of *PREX1* and was the only *PREX1*-dependent non-AML line (Figure 6B). Though PREX1 and TIAM1 share little sequence homology (6% amino acid identity), we posited that they might nonetheless be functionally interchangeable. To test this idea, we screened the focused library in THP-1 cells stably expressing TIAM1. As compared to the parental line, THP1-TIAM1 cells have a reduced dependence on *PREX1*, which showed the greatest change in CS of all 132 genes screened (Figures 7B and 7C). Additionally, *TIAM1* expression rescued the decrease in PAK signaling caused by
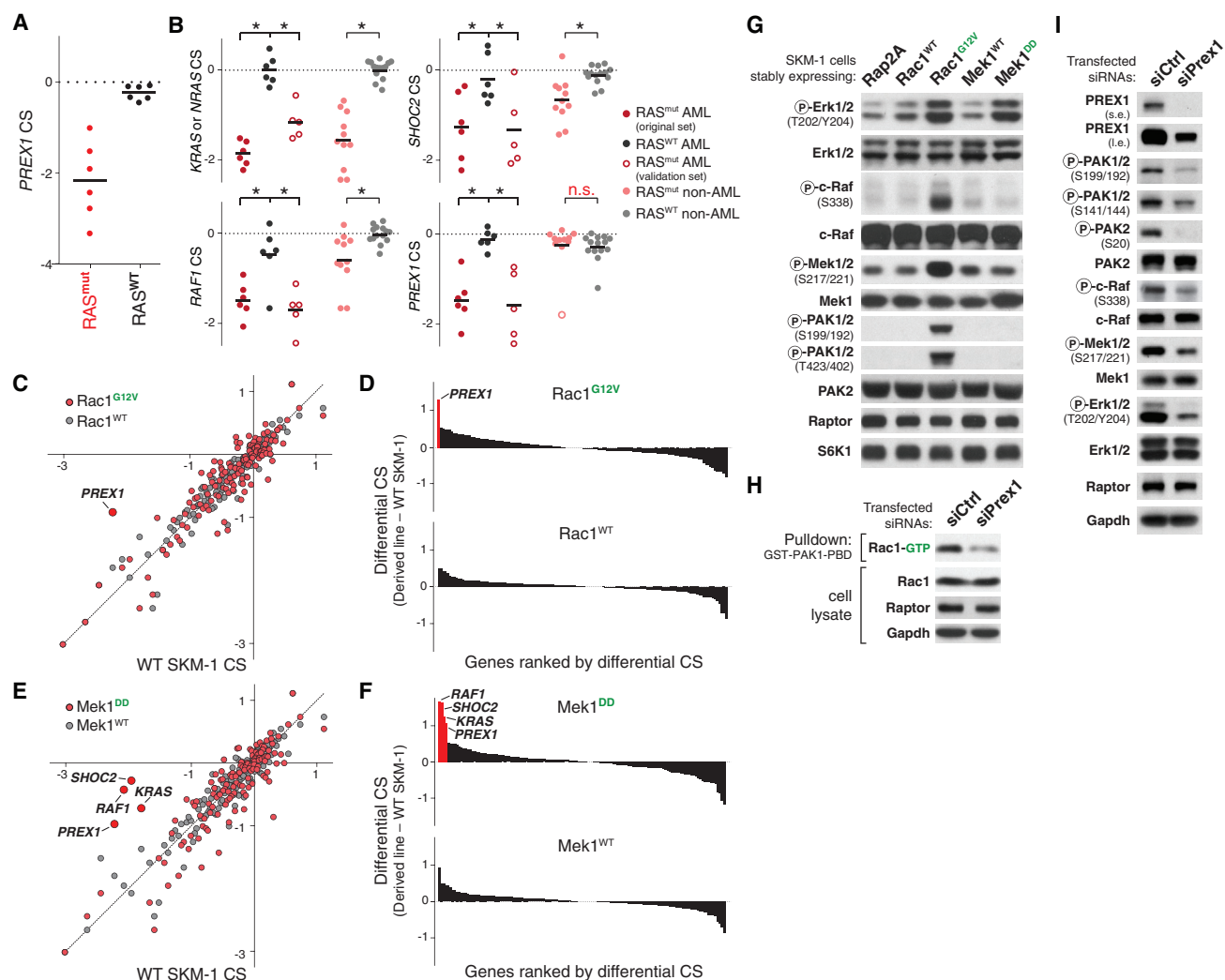
Figure 6. MAPK Pathway Activation Requires *PREX1* in Mutant Ras AML Cells

(A) *PREX1* is differentially essential between human AML cell lines with mutant and wild-type Ras.

(B) Focused library screens in 42 human hematopoietic cancer cell lines. The mutant Ras, non-AML cell line in the *PREX1* CS plot represented by the open circle is NU-DHL-1 (see Figure 7A). *p < 0.05, Welch's t test.

(C–F) Focused library screens in SKM-1 cells stably expressing (C and D) wild-type and constitutively active Rac1 (Rac1[G12V]) (E and F), wild-type, constitutively active Mek1 (Mek1[DD]), and the parental SKM-1 line.

(G) Mek1 activation increases phospho-Erk1/2 levels. Rac1 activation results in increased phospho-PAK levels and MAPK pathway activity. SKM-1 Rap2A served as a negative control. Raptor and S6K1 were used as loading controls.

(H and I) *PREX1* knockdown reduces (H) active Rac1, (I) phospho-PAK, and MAPK pathway activity. Raptor and GAPDH served as loading controls. s.e., short exposure. l.e., long exposure.

See also Figure S6 and Tables S1, S2, S3, S6, S7, and S8.

PREX1 loss (Figure 7D). Thus, we conclude that Ras-driven AML cells specifically require *PREX1* because it is the only active Rac-GEF expressed in this cancer subtype.

While *PREX1* may not serve as an ideal target for pharmacological inhibition, our findings raise the possibility that AML and non-AML cancers driven by oncogenic Ras may be sensitive to inhibition of the group I PAKs (PAK1-3). Using FRAX-597, a small-molecule inhibitor of multiple kinases including the group I PAKs, we tested this hypothesis in two isogenic cell pairs with differential requirements for Ras signaling: SKM-1

cells expressing either Mek1[DD] or the control protein Rap2A, as well as CGN Ba/F3 cells cultured in the presence or absence of IL-3. In both cases, the cells dependent on Ras signaling were more sensitive to PAK inhibition than the isogenic control cells even though FRAX-597 inhibits many other kinases besides the PAKs (Figure 7E) (Chow et al., 2012). Collectively, these results suggest a model in which all Ras-driven cancers require PAK activity in order to fully activate MAPK signaling, with each cancer subtype activating the PAKs via distinct mechanisms (Figure 7F).
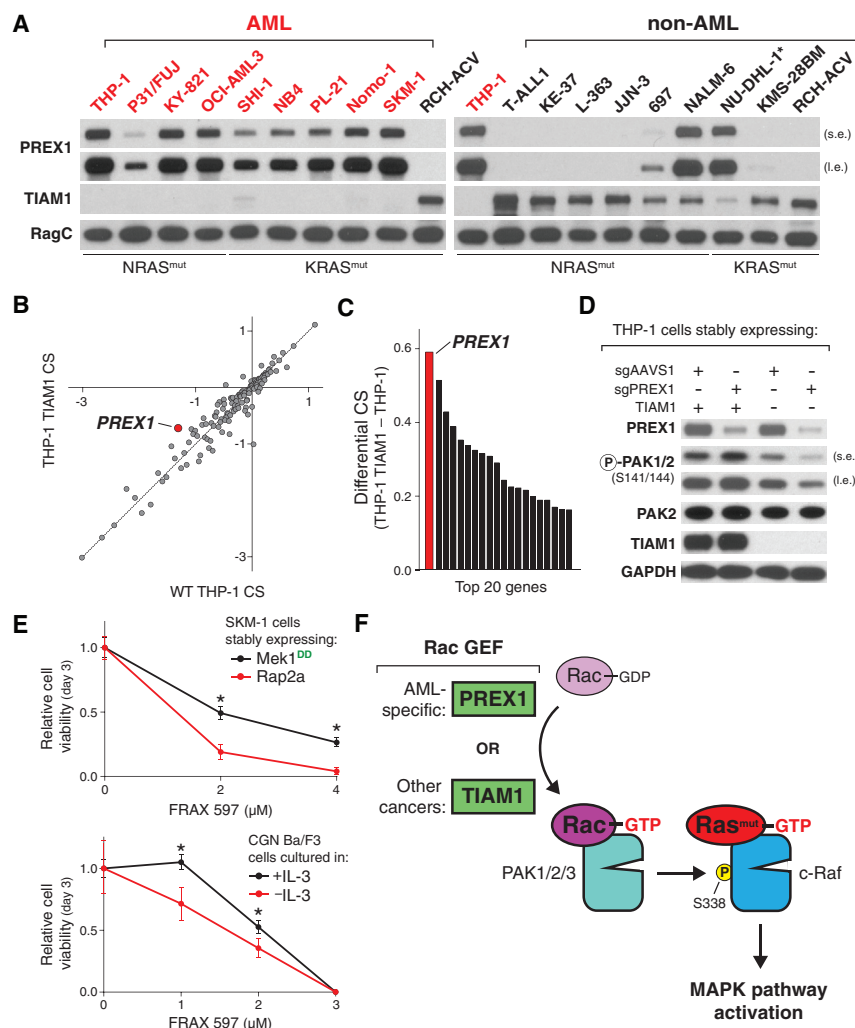
Figure 7. Lack of Paralog Expression Explains _PREX1_-Dependence in AML

(A) Analysis of PREX1 and TIAM1 expression. RagC was used as a loading control.

(B) Focused library screens in wild-type and TIAM1-overexpressing THP-1 cells.

(C) CRISPR scores from THP-1 TIAM1 cells are compared with those of the parental THP-1 cells to calculate the differential CS.

(D) _TIAM1_ rescues sgPREX1-mediated inhibition of PAK signaling in THP-1 cells. GAPDH served as a loading control.

(E) Treatment of isogenic SKM-1 and Ba/F3 cell line pairs with a group I PAK inhibitor FRAX-597. Error bars represent SD from ten replicate wells. *p < 0.05, Welch's t test.

(F) Proposed model of cell-type-specific _PREX1_ dependence.

SE, short exposure; LE, long exposure.

See also Tables S6, S7, and S8.

cells from those solely involved in tumor initiation. Even for cells harboring activating mutations in the same oncogene, we found differences in essentiality (only three of four _FLT3_ mutant lines required _FLT3_). Thus, to more accurately guide cancer treatment, functional testing of patient tumor cells, should be considered in combination with sequence analysis.

Functional Gene Network Mapping Using Correlated Gene Essentiality Analysis

The natural variability in the genetic and epigenetic makeup across human cancer cell lines leads to differences in gene essentiality and so provides a convenient means for defining functional gene networks. Even between lines of a single subtype, we found many genes with variable essentiality. Reasoning that genes in the same biological pathway should show similar patterns of essentiality, we used the CRISPR scores to cluster genes into groups with correlated essentiality. Interestingly, the scores of many gene pairs correlated linearly, with the different cell lines showing graded, rather than binary levels of requirements for the genes. Our analysis uncovered several classes of functional relationships including gene sets encoding protein complexes, metabolic pathways, and enzyme-substrate pairs and enabled us to determine the molecular functions of uncharacterized genes.

Analysis of other cancer types or across cancer types may reveal additional interactions and surveying across media conditions or in the presence of chemical compounds may also yield valuable insights. Moreover, we anticipate that more sophisticated analysis of our dataset using approaches that can detect multi-way interactions will allow for continued discovery.

With the exception of the genes involved in p53 signaling, the basis of the variable essentiality of all other gene clusters

DISCUSSION

An Integrative Genomic Approach Reveals Oncogene Dependency

Cancer genome sequencing efforts have provided an increasingly complete catalog of the genes altered during tumor development (Lawrence et al., 2014). Functional studies enable a direct assessment of the contribution of each of these genes to cancer cell fitness (Boehm and Hahn, 2011; Garraway and Lander, 2013). Together, these complementary approaches should accelerate the identification of novel oncogenes and potential therapeutic targets. Some cancers are driven by rare events that are difficult to distinguish from random mutations and thus require functional analysis to assess the significance of an alteration (Berger et al., 2016; Starita et al., 2015; Tsang et al., 2016). For instance, the tiled design of our libraries enabled us to identify the essentiality of translocation events including a rare inversion involving the _RAF1_ kinase in OCI-AML2 cells.

However, mutational information alone cannot discriminate between oncogenes required for the continued growth of cancer

remains unclear. Such an understanding will be required in order to exploit these pathways for cancer therapy. Similar to efforts to predict cancer drug response, integrative approaches may help uncover biomarkers for gene essentiality.

Screens in Established Human AML and Engineered Mouse Cell Lines Uncover a Common Set of Ras Synthetic Lethal Interactions

We focused on a special case of co-essentiality: synthetic lethality with oncogenic Ras. In large part, our study suggests that the development of therapies that selectively impact Ras-dependent cancer cells will require re-focusing efforts on targeting select components of the Ras pathway itself.

Ras, like many small GTPases, undergoes a series of post-translational modifications to facilitate interaction with the inner leaflet of the plasma membrane. Efforts to block this process have been primarily directed toward inhibition of the initial step of the pathway catalyzed by FTase (Cox et al., 2014). However, FTase inhibitors have been ineffective in the clinic as Kras and Nras can be geranylgeranylated, an alternative prenylation pathway (Whyte et al., 1997). Additionally, our results here and from prior screens conducted in other cancer subtypes indicate that FTase is required in all cells. In contrast to FTase, the enzymes catalyzing the latter two steps of the Ras processing pathway, Rce1 and Icmt, do display synthetic lethality with oncogenic Ras and may thus serve as therapeutic targets.

Our results provide further support for the central role of MAPK signaling in Ras-driven cancers and suggest c-Raf as a therapeutic target. The unique requirement for c-Raf, but not other Raf kinases, is consistent with only c-Raf being required in lung cancer models driven by oncogenic Ras (Blasco et al., 2011; Karreth et al., 2011).

A mechanistic insight from our study is the critical role of the Rac/PAK signaling axis in promoting MAPK activity in mutant Ras cancers. Even though the Rac GTPases activate many downstream pathways, we found that forced expression of constitutively active Mek1 can bypass the requirement for *PREX1*. The selective essentiality of *PREX1* in Ras-driven AML, but not in the other cancer types tested, likely reflects the critical role of *PREX1* in normal myeloid cells. In neutrophils, where *PREX1* is highly expressed, host- and pathogen-derived chemotactic factors trigger activation of the PI3-Kγ and GPCR pathways (Welch et al., 2002). This results in the generation of PIP$_3$ and free Gβγ subunits which recruit PREX1 and stimulate Rac-GEF activity. In AML cells, Gβγ and PIP$_3$ may be similarly required to activate PREX1. We note that genes encoding two Gβ subunits (*GNB1/2*), a Gγ subunit (*GNG5*), a Gβγ-modulator (*PDCL*), and the catalytic and regulatory subunits of PI3-Kγ (*PIK3CG/PIK3R5*) all showed partial Ras co-dependency (Figure S5A). We hypothesize that Ras-driven cancers originating from other cell types rely on other Rac-GEFs, such as TIAM1 and VAV1, to activate PAK signaling.

Design of Synthetic Lethal Screens and sgRNA Libraries

The combination of screening approaches employed here provides a guide for the design of robust screens for synthetic lethal interactions. As illustrated by the case *PREX1* in Ras-driven AML, genetic interactions with oncogenes may occur in a cell context-dependent manner. Thus, it may be sensible to screen lines of a particular cell type or to include enough cell lines representing each cancer type. Additionally, screens across isogenic cell lines should be employed to eliminate factors that may confound analyses across genetically heterogeneous cancer cell lines. Here, we screened Ba/F3 cells expressing oncogenic *NRAS* in the presence and absence of IL-3. This perturbation altered oncogene dependence, but not proliferation rate (Figure S5C).

Microarray-based oligonucleotide synthesis enables the rapid generation of focused sgRNA libraries for follow-up studies. As such experiments require vastly fewer numbers of cells, many additional cell lines can be tested. By using expanded cell line panels representing more cancer types, the generality of the interactions can be assessed and with engineered panels of lines, epistatic relationships between hit genes defined. Moreover, it may be possible to conduct screens using murine cancer models and identify genes that play critical roles in vivo.

General Comments on Synthetic Lethality in Cancer

Synthetic lethal interactions in cancer cells can, in principle, occur between several classes of genes. The prototypical example is the inactivation of a so-called 'caretaker' gene involved in the maintenance of genomic stability that leads to dependence on a parallel maintenance pathway (Ashworth et al., 2011; Kaelin, 2005). Such interactions may arise between genes involved in distinct but functionally overlapping processes, as seen with the BRCA and PARP DNA repair pathways, or between highly related and perhaps even interchangeable paralogs, such as *ARID1A* and *ARID1B* (Farmer et al., 2005). However, this paradigm may not apply to Ras and other genes involved in signal transduction. In contrast to loss-of-function mutations in caretaker genes, oncogenic mutations in growth factor signaling pathways result in hyperactive signaling and, in most cases, render cells dependent on the altered pathway (Luo et al., 2009b). Furthermore, as these mutations act in a dominant fashion, they are typically found in the heterozygous state, leaving the wild-type allele intact.

Genes and pathways that protect cancer cells from the diverse stresses associated with the malignant state represent a second class of potential vulnerabilities. In comparison to their normal counterparts, cancer cells rely to a much greater extent on such cytoprotective pathways as they experience elevated levels of mitotic, oxidative, proteotoxic, metabolic, and DNA damage-related stress (Luo et al., 2009b). While many of these stresses can be experimentally induced by the expression of specific oncogenes, they are almost universally found in established tumors regardless of genotype (Courtois-Cox et al., 2008). Thus, it is unclear whether these liabilities can be linked to any particular oncogene per se or if they arise as a secondary consequence of the increased genomic instability and mitotic index characteristic of all cancer cells. Indeed, chaperones, such as Hsp90, act as "genetic hubs" and show epistasis with hundreds of client proteins, including several oncogenic kinases (Whitesell and Lindquist, 2005). More comprehensive studies that compare various genetically defined malignant and pre-malignant cells are needed to

pinpoint the specific features of the oncogenic state that sensitize cells to inhibition of individual stress response pathways. Importantly, as full inhibition of many of these pathways is likely to be lethal, gene knockdown approaches, such as CRISPRi, may be better suited to interrogate them (Gilbert et al., 2014; Horlbeck et al., 2016).

The only consistent differences in gene essentiality between the mutant and wild-type Ras cells in our study were in genes closely connected to Ras itself (Ras post-translational processing and MAPK signaling). Extensive experimental evidence in Ras-driven cell lines and in murine cancer models supports the importance of these pathways. Our data are in general agreement with findings from our correlated essentiality analysis—as with other pathways and complexes, cells that require Ras also require other genes that act in concert with Ras to promote survival and proliferation. We anticipate that screens for synthetic lethal partners of other driver oncogenes will uncover similar networks of ancillary genes that may serve as attractive targets for therapy. More broadly, through the systematic application of CRISPR-based screens, it should be possible to comprehensively identify the acquired vulnerabilities of human cancers.

STAR★METHODS

Detailed methods are provided in the online version of this paper and include the following:

- KEY RESOURCES TABLE
- CONTACT FOR REAGENT AND RESOURCE SHARING
- EXPERIMENTAL MODEL AND SUBJECT DETAILS
    - Cell Lines and Genomic Annotations
    - Cell Culture Conditions
- METHOD DETAILS
    - Virus Production and Transduction
    - Vector Construction
    - Generation of Isogenic Cell Lines for CRISPR Screening
    - Genome-wide CRISPR Screening
    - Genome-wide sgRNA Library Construction
    - Secondary CRISPR Screening
    - Antibodies
    - Cell Lysis and Immunoblotting
    - Immunoprecipitation Studies
    - Immunofluorescence
    - Seahorse Analysis
    - siRNA Experiments
    - RNA Sequencing
    - Short-Term Proliferation Assays
    - Sanger Sequencing
- QUANTIFICATION AND STATISTICAL ANALYSIS
    - Genome-wide CRISPR Screening
    - Secondary CRISPR Screening
    - Comparative Essentiality Testing
    - Copy Number Peak Analysis
    - Correlated Gene Essentiality Analysis
- DATA AND SOFTWARE AVAILABILITY
    - Data Resources

REFERENCES

Aguirre, A.J., Meyers, R.M., Weir, B.A., Vazquez, F., Zhang, C.-Z., Ben-David, U., Cook, A., Ha, G., Harrington, W.F., Doshi, M.B., et al. (2016). Genomic copy number dictates a gene-independent cell response to CRISPR-Cas9 targeting (Cancer Disc). http://dx.doi.org/10.1158/2159-8290.CD-16-0154.

Ashworth, A., Lord, C.J., and Reis-Filho, J.S. (2011). Genetic interactions in cancer progression and treatment. Cell 145, 30–38.

Barbie, D.A., Tamayo, P., Boehm, J.S., Kim, S.Y., Moody, S.E., Dunn, I.F., Schinzel, A.C., Sandy, P., Meylan, E., Scholl, C., et al. (2009). Systematic RNA interference reveals that oncogenic KRAS-driven cancers require TBK1. Nature 462, 108–112.

Barretina, J., Caponigro, G., Stransky, N., Venkatesan, K., Margolin, A.A., Kim, S., Wilson, C.J., Lehár, J., Kryukov, G.V., Sonkin, D., et al. (2012). The Cancer Cell Line Encyclopedia enables predictive modelling of anticancer drug sensitivity. Nature 483, 603–607.

Bassi, D.E., Fu, J., Lopez de Cicco, R., and Klein-Szanto, A.J.P. (2005). Proprotein convertases: "master switches" in the regulation of tumor growth and progression. Mol. Carcinog. 44, 151–161.

Berger, A.H., Brooks, A.N., Wu, X., Shrestha, Y., Chouinard, C., Piccioni, F., Bagul, M., Kamburov, A., Imielinski, M., Hogstrom, L., et al. (2016). High-throughput Phenotyping of Lung Cancer Somatic Mutations. Cancer Cell 30, 214–228.

Blasco, Rafael B., Francoz, S., Santamaría, D., Cañamero, M., Dubus, P., Charron, J., Baccarini, M., and Barbacid, M. (2011). c-Raf, but not B-Raf, is essential for development of K-Ras oncogene-driven non-small cell lung carcinoma. Cancer Cell 19, 652–663.

Boehm, J.S., and Hahn, W.C. (2011). Towards systematic functional characterization of cancer genomes. Nat. Rev. Genet. 12, 487–498.

Chantranupong, L., Scaria, S.M., Saxton, R.A., Gygi, M.P., Shen, K., Wyant, G.A., Wang, T., Harper, J.W., Gygi, S.P., and Sabatini, D.M. (2016). The

CASTOR proteins are arginine sensors for the mTORC1 pathway. Cell *165*, 153–164.

Chen, C., Itakura, E., Weber, K.P., Hegde, R.S., and de Bono, M. (2014). An ER complex of ODR-4 and ODR-8/Ufm1 specific protease 2 promotes GPCR maturation by a Ufm1-independent mechanism. PLoS Genet. *10*, e1004082.

Cheung, H.W., Cowley, G.S., Weir, B.A., Boehm, J.S., Rusin, S., Scott, J.A., East, A., Ali, L.D., Lizotte, P.H., Wong, T.C., et al. (2011). Systematic investigation of genetic vulnerabilities across cancer cell lines reveals lineage-specific dependencies in ovarian cancer. Proc. Natl. Acad. Sci. USA *108*, 12372–12377.

Chow, H.Y., Jubb, A.M., Koch, J.N., Jaffer, Z.M., Stepanova, D., Campbell, D.A., Duron, S.G., O'Farrell, M., Cai, K.Q., Klein-Szanto, A.J.P., et al. (2012). p21-Activated kinase 1 is required for efficient tumor formation and progression in a Ras-mediated skin cancer model. Cancer Res. *72*, 5966–5975.

Cong, L., Ran, F.A., Cox, D., Lin, S., Barretto, R., Habib, N., Hsu, P.D., Wu, X., Jiang, W., Marraffini, L.A., and Zhang, F. (2013). Multiplex genome engineering using CRISPR/Cas systems. Science *339*, 819–823.

Cordeddu, V., Di Schiavi, E., Pennacchio, L.A., Ma'ayan, A., Sarkozy, A., Fodale, V., Cecchetti, S., Cardinale, A., Martin, J., Schackwitz, W., et al. (2009). Mutation of SHOC2 promotes aberrant protein N-myristoylation and causes Noonan-like syndrome with loose anagen hair. Nat. Genet. *41*, 1022–1026.

Costanzo, M., VanderSluis, B., Koch, E.N., Baryshnikova, A., Pons, C., Tan, G., Wang, W., Usaj, M., Hanchard, J., Lee, S.D., et al. (2016). A global genetic interaction network maps a wiring diagram of cellular function. Science *353*, pii: aaf1420.

Courtois-Cox, S., Jones, S.L., and Cichowski, K. (2008). Many roads lead to oncogene-induced senescence. Oncogene *27*, 2801–2809.

Cowley, G.S., Weir, B.A., Vazquez, F., Tamayo, P., Scott, J.A., Rusin, S., East-Seletsky, A., Ali, L.D., Gerath, W.F.J., Pantel, S.E., et al. (2014). Parallel genome-scale loss of function screens in 216 cancer cell lines for the identification of context-specific genetic dependencies. Sci. Data *1*, 140035.

Cox, A.D., Fesik, S.W., Kimmelman, A.C., Luo, J., and Der, C.J. (2014). Drugging the undruggable RAS: Mission possible? Nat. Rev. Drug Discov. *13*, 828–851.

Ebi, H., Costa, C., Faber, A.C., Nishtala, M., Kotani, H., Juric, D., Della Pelle, P., Song, Y., Yano, S., Mino-Kenudson, M., et al. (2013). PI3K regulates MEK/ERK signaling in breast cancer via the Rac-GEF, P-Rex1. Proc. Natl. Acad. Sci. USA *110*, 21124–21129.

Farmer, H., McCabe, N., Lord, C.J., Tutt, A.N.J., Johnson, D.A., Richardson, T.B., Santarosa, M., Dillon, K.J., Hickson, I., Knights, C., et al. (2005). Targeting the DNA repair defect in BRCA mutant cells as a therapeutic strategy. Nature *434*, 917–921.

Feig, L.A., and Cooper, G.M. (1988). Relationship among guanine nucleotide exchange, GTP hydrolysis, and transforming potential of mutated ras proteins. Mol. Cell. Biol. *8*, 2472–2478.

Floyd, B.J., Wilkerson, E.M., Veling, M.T., Minogue, C.E., Xia, C., Beebe, E.T., Wrobel, R.L., Cho, H., Kremer, L.S., Alston, C.L., et al. (2016). Mitochondrial protein interaction mapping identifies regulators of respiratory chain function. Mol. Cell *63*, 621–632.

Forbes, S.A., Beare, D., Gunasekaran, P., Leung, K., Bindal, N., Boutselakis, H., Ding, M., Bamford, S., Cole, C., Ward, S., et al. (2015). COSMIC: exploring the world's knowledge of somatic mutations in human cancer. Nucleic Acids Res. *43*, D805–D811.

Garnett, M.J., Edelman, E.J., Heidorn, S.J., Greenman, C.D., Dastur, A., Lau, K.W., Greninger, P., Thompson, I.R., Luo, X., Soares, J., et al. (2012). Systematic identification of genomic markers of drug sensitivity in cancer cells. Nature *483*, 570–575.

Garraway, L.A., and Lander, E.S. (2013). Lessons from the cancer genome. Cell *153*, 17–37.

Giaever, G., Chu, A.M., Ni, L., Connelly, C., Riles, L., Véronneau, S., Dow, S., Lucau-Danila, A., Anderson, K., André, B., et al. (2002). Functional profiling of the Saccharomyces cerevisiae genome. Nature *418*, 387–391.

Gibson, D.G., Young, L., Chuang, R.Y., Venter, J.C., Hutchison, C.A., 3rd, and Smith, H.O. (2009). Enzymatic assembly of DNA molecules up to several hundred kilobases. Nat. Methods *6*, 343–345.

Gilbert, L.A., Horlbeck, M.A., Adamson, B., Villalta, J.E., Chen, Y., Whitehead, E.H., Guimaraes, C., Panning, B., Ploegh, H.L., Bassik, M.C., et al. (2014). Genome-scale CRISPR-mediated control of gene repression and activation. Cell *159*, 647–661.

Hart, T., Chandrashekhar, M., Aregger, M., Steinhart, Z., Brown, K.R., MacLeod, G., Mis, M., Zimmermann, M., Fradet-Turcotte, A., Sun, S., et al. (2015). High-resolution CRISPR screens reveal fitness genes and genotype-specific cancer liabilities. Cell *163*, 1515–1526.

Horlbeck, M.A., Gilbert, L.A., Villalta, J.E., Adamson, B., Pak, R.A., Chen, Y., Fields, A.P., Park, C.Y., Corn, J.E., Kampmann, M., and Weissman, J.S. (2016). Compact and highly active next-generation libraries for CRISPR-mediated gene repression and activation. eLife *5*, e19760.

Hughes, T.R., Marton, M.J., Jones, A.R., Roberts, C.J., Stoughton, R., Armour, C.D., Bennett, H.A., Coffey, E., Dai, H., He, Y.D., et al. (2000). Functional discovery via a compendium of expression profiles. Cell *102*, 109–126.

Kaelin, W.G., Jr. (2005). The concept of synthetic lethality in the context of anticancer therapy. Nat. Rev. Cancer *5*, 689–698.

Karreth, F.A., Frese, K.K., DeNicola, G.M., Baccarini, M., and Tuveson, D.A. (2011). C-Raf is required for the initiation of lung cancer by K-Ras$^{(G12D)}$. Cancer Discov. *1*, 128–136.

Kim, H.S., Mendiratta, S., Kim, J., Pecot, C.V., Larsen, J.E., Zubovych, I., Seo, B.Y., Kim, J., Eskiocak, B., Chung, H., et al. (2013). Systematic identification of molecular subtype-selective vulnerabilities in non-small-cell lung cancer. Cell *155*, 552–566.

King, A.J., Sun, H., Diaz, B., Barnard, D., Miao, W., Bagrodia, S., and Marshall, M.S. (1998). The protein kinase Pak3 positively regulates Raf-1 activity through phosphorylation of serine 338. Nature *396*, 180–183.

Klijn, C., Durinck, S., Stawiski, E.W., Haverty, P.M., Jiang, Z., Liu, H., Degenhardt, J., Mayba, O., Gnad, F., Liu, J., et al. (2015). A comprehensive transcriptional portrait of human cancer cell lines. Nat. Biotechnol. *33*, 306–312.

Koike-Yusa, H., Li, Y., Tan, E.P., Velasco-Herrera, Mdel.C., and Yusa, K. (2014). Genome-wide recessive genetic screening in mammalian cells with a lentiviral CRISPR-guide RNA library. Nat. Biotechnol. *32*, 267–273.

Komatsu, M., Chiba, T., Tatsumi, K., Iemura, S., Tanida, I., Okazaki, N., Ueno, T., Kominami, E., Natsume, T., and Tanaka, K. (2004). A novel protein-conjugating system for Ufm1, a ubiquitin-fold modifier. EMBO J. *23*, 1977–1986.

Lawrence, M.S., Stojanov, P., Mermel, C.H., Robinson, J.T., Garraway, L.A., Golub, T.R., Meyerson, M., Gabriel, S.B., Lander, E.S., and Getz, G. (2014). Discovery and saturation analysis of cancer genes across 21 tumour types. Nature *505*, 495–501.

Lehrbach, N.J., and Ruvkun, G. (2016). Proteasome dysfunction triggers activation of SKN-1A/Nrf1 by the aspartic protease DDI-1. eLife *5*, e17721.

Luo, J., Emanuele, M.J., Li, D., Creighton, C.J., Schlabach, M.R., Westbrook, T.F., Wong, K.-K., and Elledge, S.J. (2009a). A genome-wide RNAi screen identifies multiple synthetic lethal interactions with the Ras oncogene. Cell *137*, 835–848.

Luo, J., Solimini, N.L., and Elledge, S.J. (2009b). Principles of cancer therapy: oncogene and non-oncogene addiction. Cell *136*, 823–837.

Marcotte, R., Brown, K.R., Suarez, F., Sayad, A., Karamboulas, K., Krzyzanowski, P.M., Sircoulomb, F., Medrano, M., Fedyshyn, Y., Koh, J.L.Y., et al. (2012). Essential gene profiles in breast, pancreatic, and ovarian cancer cells. Cancer Discov. *2*, 172–189.

Munoz, D.M., Cassiani, P.J., Li, L., Billy, E., Korn, J.M., Jones, M.D., Golji, J., Ruddy, D.A., Yu, K., McAllister, G., et al. (2016). CRISPR screens provide a comprehensive assessment of cancer vulnerabilities but generate false-positive hits for highly amplified genomic regions. Cancer Discov. *6*, 900–913.

Quentmeier, H., Reinhardt, J., Zaborski, M., and Drexler, H.G. (2003). FLT3 mutations in acute myeloid leukemia cell lines. Leukemia *17*, 120–124.

Quentmeier, H., MacLeod, R.A.F., Zaborski, M., and Drexler, H.G. (2006). JAK2 V617F tyrosine kinase mutation in cell lines derived from myeloproliferative disorders. Leukemia *20*, 471–476.

Radhakrishnan, S.K., den Besten, W., and Deshaies, R.J. (2014). p97-dependent retrotranslocation and proteolytic processing govern formation of active Nrf1 upon proteasome inhibition. eLife *3*, e01856.

Rodriguez-Viciana, P., Oses-Prieto, J., Burlingame, A., Fried, M., and McCormick, F. (2006). A phosphatase holoenzyme comprised of Shoc2/Sur8 and the catalytic subunit of PP1 functions as an M-Ras effector to modulate Raf activity. Mol. Cell *22*, 217–230.

Schlabach, M.R., Luo, J., Solimini, N.L., Hu, G., Xu, Q., Li, M.Z., Zhao, Z., Smogorzewska, A., Sowa, M.E., Ang, X.L., et al. (2008). Cancer proliferation gene discovery through functional genomics. Science *319*, 620–624.

Shalem, O., Sanjana, N.E., Hartenian, E., Shi, X., Scott, D.A., Mikkelsen, T.S., Heckl, D., Ebert, B.L., Root, D.E., Doench, J.G., and Zhang, F. (2014). Genome-scale CRISPR-Cas9 knockout screening in human cells. Science *343*, 84–87.

Starita, L.M., Young, D.L., Islam, M., Kitzman, J.O., Gullingsrud, J., Hause, R.J., Fowler, D.M., Parvin, J.D., Shendure, J., and Fields, S. (2015). Massively parallel functional analysis of BRCA1 RING domain variants. Genetics *200*, 413–422.

Subramanian, A., Tamayo, P., Mootha, V.K., Mukherjee, S., Ebert, B.L., Gillette, M.A., Paulovich, A., Pomeroy, S.L., Golub, T.R., Lander, E.S., and Mesirov, J.P. (2005). Gene set enrichment analysis: a knowledge-based approach for interpreting genome-wide expression profiles. Proc. Natl. Acad. Sci. USA *102*, 15545–15550.

Swarthout, J.T., Lobo, S., Farh, L., Croke, M.R., Greentree, W.K., Deschenes, R.J., and Linder, M.E. (2005). DHHC9 and GCP16 constitute a human protein fatty acyltransferase with specificity for H- and N-Ras. J. Biol. Chem. *280*, 31141–31148.

Toledo, C.M., Ding, Y., Hoellerbauer, P., Davis, R.J., Basom, R., Girard, E.J., Lee, E., Corrin, P., Hart, T., Bolouri, H., et al. (2015). Genome-wide CRISPR-Cas9 screens reveal loss of redundancy between PKMYT1 and WEE1 in glioblastoma stem-like cells. Cell Rep. *13*, 2425–2439.

Trapnell, C., Roberts, A., Goff, L., Pertea, G., Kim, D., Kelley, D.R., Pimentel, H., Salzberg, S.L., Rinn, J.L., and Pachter, L. (2012). Differential gene and transcript expression analysis of RNA-seq experiments with TopHat and Cufflinks. Nat Protoc. *7*, 562–578.

Tsang, Y.H., Dogruluk, T., Tedeschi, P.M., Wardwell-Ozgo, J., Lu, H., Espitia, M., Nair, N., Minelli, R., Chong, Z., Chen, F., et al. (2016). Functional annotation of rare gene aberration drivers of pancreatic cancer. Nat. Commun. *7*, 10500.

Tzelepis, K., Koike-Yusa, H., De Braekeleer, E., Li, Y., Metzakopian, E., Dovey, O.M., Mupo, A., Grinkevich, V., Li, M., Mazan, M., et al. (2016). A CRISPR dropout screen identifies genetic vulnerabilities and therapeutic targets in acute myeloid leukemia. Cell Rep. *17*, 1193–1205.

Wang, T., Wei, J.J., Sabatini, D.M., and Lander, E.S. (2014). Genetic screens in human cells using the CRISPR-Cas9 system. Science *343*, 80–84.

Wang, T., Birsoy, K., Hughes, N.W., Krupczak, K.M., Post, Y., Wei, J.J., Lander, E.S., and Sabatini, D.M. (2015). Identification and characterization of essential genes in the human genome. Science *350*, 1096–1101.

Welch, H.C.E., Coadwell, W.J., Ellson, C.D., Ferguson, G.J., Andrews, S.R., Erdjument-Bromage, H., Tempst, P., Hawkins, P.T., and Stephens, L.R. (2002). P-Rex1, a PtdIns(3,4,5)P3- and Gbetagamma-regulated guanine-nucleotide exchange factor for Rac. Cell *108*, 809–821.

Whitesell, L., and Lindquist, S.L. (2005). HSP90 and the chaperoning of cancer. Nat. Rev. Cancer *5*, 761–772.

Whyte, D.B., Kirschmeier, P., Hockenberry, T.N., Nunez-Oliva, I., James, L., Catino, J.J., Bishop, W.R., and Pai, J.K. (1997). K- and N-Ras are geranylgeranylated in cells treated with farnesyl protein transferase inhibitors. J. Biol. Chem. *272*, 14459–14464.

STAR★METHODS

KEY RESOURCES TABLE

REAGENT or RESOURCE	SOURCE	IDENTIFIER
Antibodies		
Mouse monoclonal anti-HA (clone 6E2)	Cell Signaling Technology	2367
Rabbit polyclonal anti-HA	Bethyl	A190-208A
Rabbit monoclonal anti-FLAG (clone D6W5B)	Cell Signaling Technology	14793
Rabbit monoclonal anti-COX IV (clone 3E11)	Cell Signaling Technology	4850
Total OXPHOS human WB Antibody Cocktail	Abcam	ab110411
Rabbit polyclonal anti-Raptor	EMD Millipore	09-217
Rabbit monoclonal anti-UFM1 [clone EPR4264(2)]	Abcam	ab109305
Mouse monoclonal anti-GAPDH (clone GT239)	GeneTex	GTX627408
Rabbit monoclonal anti-PREX1 (clone D8O8D)	Cell Signaling Technology	13168
Mouse monoclonal anti-Sur-8 (clone D-8)	Santa Cruz	sc-514779
Rabbit polyclonal anti-Tiam1 (C-16)	Santa Cruz	sc-872
Rabbti polyclonal RagC	Cell Signaling Technology	3360
Rabbit polyclonal anti-Phospho-PAK1 (Ser144)/PAK2 (Ser141)	Cell Signaling Technology	2606
Rabbit monoclonal anti-Phospho-PAK2 (Ser20) [clone EPR658(2)]	Abcam	ab76419
Rabbit polyclonal anti-PAK2	Cell Signaling Technology	2608
Rabbit monoclonal anti-Phospho-p44/42 MAPK (Erk1/2) (Thr202/Tyr204) (clone D13.14.4E)	Cell Signaling Technology	4370
Rabbit polyclonal anti-ERK1/2 p44/42 MAPK (Erk1/2)	Cell Signaling Technology	9102
Rabbit monoclonal anti-Phospho-c-Raf (Ser338) (clone 56A6)	Cell Signaling Technology	9427
Rabbit polyclonal anti-c-Raf	Cell Signaling Technology	9422
Rabbit monoclonal anti-Phospho-MEK1/2 (Ser217/221) (clone 41G9)	Cell Signaling Technology	9154
Mouse monoclonal anti-MEK1 (clone 61B12)	Cell Signaling Technology	2352
Rabbit polyclonal anti-Phospho-PAK1 (Ser199/204)/PAK2 (Ser192/197)	Cell Signaling Technology	2605
Rabbit polyclonal anti-Phospho-PAK1 (Thr423)/PAK2 (Thr402)	Cell Signaling Technology	2601
Rabbit monoclonal anti-S6 Kinase (clone 49D7)	Cell Signaling Technology	2708
Mouse monoclonal anti-UFSP2 (clone G-11)	Santa Cruz	sc-376084
Goat polyclonal anti-GRP 94 (C-19)	Santa Cruz	sc-1794
Mouse monoclonal anti-FLAG (clone M2)	Sigma-Aldrich	F1804
Goat anti-Rabbit IgG-HRP	Santa Cruz	sc-2054
Goat anti-Mouse IgG-HRP	Santa Cruz	sc-2055

Continued

REAGENT or RESOURCE	SOURCE	IDENTIFIER
Mouse monoclonal anti-rabbit IgG (Conformation Specific) (clone L27A9) (HRP Conjugate)	Cell Signaling Technology	5127
Donkey anti-Goat IgG (H+L) Secondary Antibody, Alexa Fluor 488 conjugate	Thermo Fisher Scientific	A-11055
Donkey anti-Mouse IgG (H+L) Secondary Antibody, Alexa Fluor 488 conjugate	Thermo Fisher Scientific	A-21202
Donkey anti-Mouse IgG Secondary Antibody, Alexa Fluor 568 conjugate	Thermo Fisher Scientific	A-10037
Donkey anti-Rabbit IgG (H+L) Secondary Antibody, Alexa Fluor 568 conjugate	Thermo Fisher Scientific	A-10042
Donkey anti-Mouse IgG (H+L) Secondary Antibody, Alexa Fluor 647 conjugate	Thermo Fisher Scientific	A-31571
Chemicals, Peptides, and Recombinant Proteins		
Anti-FLAG M2 Affinity Gel	Sigma-Aldrich	A2220
X-tremeGENE 9 DNA Transfection Reagent	Roche	06365787001
TaKaRa Ex Taq DNA Polymerase	TaKaRa	RR001A
Cell-Tak Cell and Tissue Adhesive	CORNING	354240
FLAG peptide (sequence DYKDDDDK)	Biopolymers Core, Koch Institute	N/A
Sodium pyruvate	Sigma-Aldrich	113-24-6
Human GM-CSF	Miltenyi Biotec	130-093-862
Recombinant murine IL-3	PeproTech	213-13
FRAX 597	Selleckchem	S7271
Ruxolitinib	Selleckchem	S1378
Selumetinib	Selleckchem	S1008
Quizartinib	LC Laboratories	Q-4747
Critical Commercial Assays		
XF24 Extracellular Flux Analyzer	Seahorse Bioscience	N/A
CellTiter-Glo Luminescent Cell Viability Assay	Promega	G7570
Active Rac1 Detection Kit	Cell Signaling Technology	8815
Nucleofector Device	Lonza	N/A
Cell Line Nucleofector Kit V	Lonza	1003
QIAamp DNA Blood Maxi Kit	QIAGEN	51192
QIAamp DNA Blood Midi Kit	QIAGEN	51183
Deposited Data		
Cell line mutational data	(Barretina et al., 2012)	https://www.broadinstitute.org/ccle
Cell line mutational data	(Forbes et al., 2015)	http://cancer.sanger.ac.uk/cell_lines
DNA copy number data	(Barretina et al., 2012)	https://www.broadinstitute.org/ccle
Cell line microarray expression data	(Barretina et al., 2012)	https://www.broadinstitute.org/ccle
Experimental Models: Cell Lines		
OCI-AML5	CCLE	ACC-247
TF-1	CCLE	ACC-334
697	CCLE	ACC-42
HPB-ALL	CCLE	ACC-483
Jurkat	CCLE	ACC-282
KE-37	CCLE	ACC-46
MOLT-16	CCLE	ACC-29
RCH-ACV	CCLE	ACC-548

(Continued on next page)

Continued

REAGENT or RESOURCE	SOURCE	IDENTIFIER
SEM	CCLE	ACC-546
SUP-T1	CCLE	ACC-140
Reh	CCLE	ACC-22
TALL-1	CCLE	ACC-521
NALM-6	CCLE	ACC-128
NB-4	CCLE	ACC-207
MOLM-13	CCLE	ACC-554
HEL	CCLE	ACC-11
PL-21	CCLE	ACC-536
MV4;11	CCLE	ACC-102
EOL-1	CCLE	ACC-386
OCI-AML2	CCLE	ACC-99
OCI-AML3	CCLE	ACC-582
P31/FUJ	CCLE	JCRB0091
MonoMac1	CCLE	ACC-252
SKM-1	CCLE	ACC-547
THP-1	CCLE	ACC-16
SHI-1	DSMZ	ACC-645
NOMO-1	J. D. Griffin	ACC-542
Ba/F3	J. D. Griffin	ACC-300
KY821	JCRB	JCRB0105
ML-2	DSMZ	ACC-15
ML-1	R. Polakiewicz	ECACC 88113007
HT	CCLE	ACC-567
KM-H2	CCLE	ACC-8
L-428	CCLE	ACC-197
MC116	CCLE	ACC-82
Mino	CCLE	ACC-687
NU-DHL-1	CCLE	ACC-583
RL	CCLE	ACC-613
SU-DHL-4	CCLE	ACC-495
U-937	CCLE	ACC-5
JJN-3	CCLE	ACC-541
KMS-26	CCLE	JCRB1187
KE-97	CCLE	RCB1435
KMS-28BM	CCLE	JCRB1192
L-363	CCLE	ACC-49
Recombinant DNA		
pLenti-Cas9-GFP	This paper	Addgene 86145
LentiCRISPR-sgC17orf89-1	This paper	Addgene 86137
LentiCRISPR-sgC17orf89-3	This paper	Addgene 86136
LentiCRISPR-sgC17orf89-2	This paper	Addgene 86135
LentiCRISPR-sgUFSP2	This paper	Addgene 86134
LentiCRISPR-sgUFM1	This paper	Addgene 86133
LentiCRISPR-sgUBA5	This paper	Addgene 86132
LentiCRISPR-sgC1orf27-2	This paper	Addgene 86131
LentiCRISPR-sgC1orf27-1	This paper	Addgene 86130
LentiCRISPR-sgSHOC2-2	This paper	Addgene 86129

Continued

REAGENT or RESOURCE	SOURCE	IDENTIFIER
LentiCRISPR-sgSHOC2-1	This paper	Addgene 86128
LentiCRISPR-sgPREX1	This paper	Addgene 86127
lentiCRISPR-AAVS1 sgRNA	(Wang et al., 2015)	Addgene 70661
pMXs3-NRAS G13D	This paper	Addgene 86144
pMXs3-TIAM1	This paper	Addgene 86143
pMXs2-MEK1 DD	This paper	Addgene 86142
pMXs2-MEK1	This paper	Addgene 86141
pMXs2-RAP2A-GFP	This paper	Addgene 86140
pMXs2-RAC1 G12V	This paper	Addgene 86139
pMXs2-RAC1	This paper	Addgene 86138
pMXs-C17orf89-FLAG	This paper	Addgene 86126
pMXs-NDUFAF5-HA	This paper	Addgene 86125
pMXs-RAP2A-GFP	This paper	Addgene 86124
pMXs-UFSP2-FLAG	This paper	Addgene 86123
pMXs-HA-C1orf27	This paper	Addgene 86122
pRK5-HA-metap2	(Chantranupong et al., 2016)	N/A
Genome-wide human sgRNA library	This paper and (Wang et al., 2015)	N/A
Genome-wide murine sgRNA library	This paper	N/A
Focused human sgRNA library	This paper	N/A
Sequence-Based Reagents		
Primers for Illumina sequencing	This paper	See the STAR Methods Genome-wide CRISPR screening
Primers for sgRNA quantification	This paper	See the STAR Methods Genome-wide CRISPR screening
Primers for genotyping KRAS	This paper	See the STAR Methods Sanger sequencing
Primers for genotyping NRAS	This paper	See the STAR Methods Sanger sequencing
Individual sgRNA target sequences	This paper	See the STAR Methods Vector construction
Genome-wide human sgRNA library	This paper and Wang et al., 2015	See Table S2
Genome-wide murine sgRNA library	This paper	See Table S4
Focused human sgRNA library	This paper	See Table S7
Software and Algorithms		
TopHat version 2.0.13	(Trapnell et al., 2012)	http://cole-trapnell-lab.github.io/cufflinks
R version 2.15.1	The R Project	https://www.r-project.org/
GSEA	(Subramanian et al., 2005)	http://software.broadinstitute.org/gsea/
Prism version 6.0.1	GraphPad	https://www.graphpad.com
python version 2.6.8	Python software foundation	https://www.python.org/

CONTACT FOR REAGENT AND RESOURCE SHARING

Requests for further information and resources may be directed to Lead Contact David M. Sabatini (sabatini@wi.mit.edu).

EXPERIMENTAL MODEL AND SUBJECT DETAILS

Cell Lines and Genomic Annotations

ML-1 cells were a gift from R. Polakiewicz of Cell Signaling Technology. Ba/F3 and Nomo-1 cells were a gift from J. D. Griffin of the Dana Farber Cancer Institute. ML-2 and SHI-1 cells were obtained from the DSMZ cell bank; KY-821 cells from the JCRB cell bank; and all other lines from the Cancer Cell Line Encyclopedia (CCLE). Genomic information was obtained from the CCLE and from the canSAR database. All cell lines obtained from the CCLE, DSMZ and JCRB were subjected to STR profiling and mycoplasma testing.

Cell Culture Conditions

All cells were cultured in IMDM (Life Technologies) and supplemented with 20% Inactivated Fetal Calf Serum (Sigma), 5 mM gluta-mine, and penicillin/streptomycin. TF-1 and OCI-AML5 cells were supplemented with 5 ng/ml human granulocyte-macrophage colony-stimulating factor (GM-CSF) (Miltenyi Biotec). Where indicated, Ba/F3 cells were supplemented with 1 ng/ml murine interleukin-3 (IL-3) (PeproTech). For pyruvate supplementation experiments, Nomo-1 cells were cultured in RPMI (US Biologicals) supplemented with 10% Inactivated Fetal Calf Serum (Sigma), 5 mM glutamine, and penicillin/streptomycin in the presence and absence of 1 mM sodium pyruvate (Sigma).

METHOD DETAILS

Virus Production and Transduction

Pseudotyped virus was produced by co-transfecting the transfer vector of interest with the VSV-G envelope plasmid and the Delta-Vpr (for lentivirus production) or Gag-Pol (for retrovirus production) packaging plasmids into HEK293T cells using XTremeGene 9 Transfection Reagent (Roche). Culture media was changed 12 hr after transfection and the virus-containing supernatant was collected 72 hr after transfection and passed through a 0.45 μm filter to eliminate cells. Target cells in 6-well tissue culture plates were infected in media containing 8 μg/mL of polybrene (EMD Millipore) by centrifugation at 2220 RPM for 45 min. 24 hr after infection, cells were pelleted to remove virus and re-plated in fresh media. When appropriate, cells were subsequently selected with antibiotics.

Vector Construction

The retroviral pMXs transfer vector was used to generate cell lines stably expressing cDNAs of interest. Several versions of the pMXs backbone vector containing different selectable markers were generated for different experiments. For studies related to C1orf27 and C17orf89, FLAG-tagged RAP2A-GFP, UFSP2, and C17orf89 and HA-tagged C1orf27 and NDUFAF5 were cloned into a vector containing blasticidin deaminase via Gibson Assembly (Gibson et al., 2009). To generate isogenic SKM-1 cell lines, RAP2A, Rac1^{WT}, Rac1^{G12V}, Mek1^{WT} (encoded by *MAP2K1*), and Mek1^{DD} (MAP2K1$^{S218D;S221D}$) were cloned into a vector containing blasticidin deaminase and TagRFP, pMXs2, via Gibson Assembly. To generate isogenic Ba/F3 and THP-1 cell lines, NRAS^{G13D} and TIAM1 were cloned into a vector containing turboRFP, pMXs3, via Gibson Assembly. To generate the Cas9-GFP expressing lentiviral construct, a version of lentiCRISPR-v1 in which the puromycin *N*-acetyltransferase ORF was replaced with eGFP.

Individual sgRNA constructs targeting were cloned into lentiCRISPR-v1 (sequences provided below) as described previously (Cong et al., 2013).

sgUFM1:	TCACGCTGACGTCGGACCCA
sgUBA5:	AAGCAGCAGAACATACTCTG
sgUFSP2:	CCAGCTGCAGGCCTATAGGA
sgC1orf27-1:	GAGATTGTGGAATTTCACAG
sgC1orf27-2:	CACAACATTACAGTGGATCC
sgC17orf89-1:	CACGCACCTGCCGTACGCCG
sgC17orf89-2:	TGTCGGCTAACGGAGCGGTG
sgC17orf89-3:	CGCGGGAGTTCGAGGCCCTG
sgSHOC2-1:	GCAGTCCCTCCCAGCAGAGG
sgSHOC2-2:	CAGTTGACCACTCTTCCCAG
sgPREX1:	GGGAGACTGCCAGACTCGGG
sgAAVS1:	GGGGCCACTAGGGACAGGAT

Generation of Isogenic Cell Lines for CRISPR Screening

For the genome-wide isogenic screens using the murine Ba/F3 cell line, cells were transduced with a lentiviral construct expressing Cas9-2A-GFP. Single, viable cells were sorted into 96-well plates by fluorescence-activated cell sorting (FACS). A sub-clone expressing high levels of GFP, termed Cas9-GFP or Ba/F3 CG, was expanded, transduced with a retroviral construct expressing NRAS^{G13D}-IRES-RFP, and subjected to FACS for RFP positive cells. During this procedure, cells were continuously passaged in the presence of IL-3 and maintained at a concentration of less than 100,000 per mL to ensure that cells did not become spontaneously cytokine-independent. To obtain cytokine-independent cells, IL-3 was withdrawn from the culture media, and, after 1 week, the surviving cells were subjected to a second round of FACS for RFP positive cells. The isolated cell population, termed Cas9-GFP NRAS^{G13D} or CGN Ba/F3, was subsequently maintained in the absence of IL-3.

For screens using the validation library, SKM-1 cells were transduced with retroviral constructs expressing Rap2A, Rac1, Rac1[G12V], Mek1 (also known as MAP2K1), and Mek1[DD]; selected with and continuously cultured in blasticidin; and subjected to two rounds of FACS for RFP positive cells. THP-1 cells were transduced with a retroviral construct expressing TIAM1 and subjected to two rounds of FACS for RFP positive cells.

Genome-wide CRISPR Screening

Genome-wide screens for all of the human and mouse cell lines was performed as described in (Wang et al., 2015) with minor modifications and the entire screening procedure was performed twice in the human NB4 and mouse Ba/F3 cells to assess reproducibility. Briefly, for each line, 240 million target cells were transduced with the viral pool to achieve an average 1000-fold coverage of the library after selection. After 72 hr, 200 million cells were selected with puromycin. An initial pool of 80 million cells was harvested for genomic DNA extraction from all of the cell lines except for THP-1 and TF-1. The remaining cells were passaged every 3 days, and after 14 doublings, a final pool of 100 million cells was harvested for genomic DNA extraction using the QIAamp DNA Blood Maxi Kit (QIAGEN)

sgRNA inserts were PCR amplified using Ex Taq DNA Polymerase (Takara) from 50-75 million genome equivalents of DNA from each initial and final sample, achieving an average coverage of ~275-400x of the sgRNA library. The resultant PCR products were purified and sequenced on a HiSeq 2500 (Illumina) (primer sequences provided below) to monitor the change in the abundance of each sgRNA between the initial and final cell populations.

Primer sequences for sgRNA quantification

Forward:

AATGATACGGCGACCACCGAGATCTACACGAATACTGCCATTTGTCTCAAGATCTA

Reverse:

CAAGCAGAAGACGGCATACGAGATCnnnnnnTTTCTTGGGTAGTTTGCAGTTTT

(nnnnnn denotes the sample barcode)

Illumina sequencing primer

CGGTGCCACTTTTTCAAGTTGATAACGGACTAGCCTTATTTTAACTTGCTATTTCTAGCTCTAAAAC

Illumina indexing primer

TTTCAAGTTACGGTAAGCATATGATAGTCCATTTTAAAACATAATTTTAAAACTGCAAACTACCCAAGAAA

Genome-wide sgRNA Library Construction

For genome-wide screens in the human AML cell lines, the human sgRNA library generated in (Wang et al., 2015) was used. Notably, the gene-targeting sgRNA sequences in our library were optimized for high cleavage activity to enable more sensitive and specific detection of cell-essential genes (Wang et al., 2015). For more complete coverage of protein-coding genes, a sub-library containing 5,401 additional sgRNAs (comprising 499 intergenic control sgRNAs and 4,902 sgRNAs targeting 497 additional protein-coding genes) were designed, synthesized, and cloned into lentiCRISPRv1. In total, the human sgRNA library contained 187,536 constructs targeting 18,543 protein-coding genes and 1,504 intergenic and non-targeting control sgRNAs.

Using similar guidelines for the design of highly specific and active sgRNAs, a genome-wide murine library containing 188,509 sgRNAs (comprising 199 intergenic control sgRNAs and 188,310 sgRNAs targeting 18,986 protein-coding genes) was designed, synthesized, and cloned into pLenti-sgRNA, a lentiviral sgRNA expression vector that does not contain Cas9.

Secondary CRISPR Screening

A pooled library containing 6,661 sgRNAs (comprising 499 intergenic control sgRNAs and 6,162 sgRNAs targeting 132 control and candidate Ras synthetic lethal genes) was designed and cloned into lentiCRISPR-v1. When possible, up to 50 sgRNAs were designed for each gene. The validation screening procedure was similar to genome-wide screens with minor modifications. 10 million cells were used for screening and harvested during the initial and final collections. Genomic DNA was extracted using QIAamp DNA Blood Midi Kit (QIAGEN) and 6 million genomic equivalents were processed for PCR.

Antibodies

The following antibodies were used for immunoblotting: HA-Tag (6E2) Mouse (Cat#2367), DYKDDDDK Tag (D6W5B) (Cat#14793), PREX1 (D8O8D) (Cat#13168), RagC (Cat#3360), p-PAK1 (S144)/PAK2 (S141) (Cat#2606), PAK2 (Cat#2608), p-MAPK (Erk1/2) (T202/Y204) (Cat#4370), MAPK (Erk1/2) (Cat#9102), p-c-Raf (S338) (56A6) (Cat#9427), c-Raf (Cat#9422), p-MEK1/2 (S217/221) (41G9) (Cat#9154), MEK1 (61B12) (Cat#2352), p-PAK1 (S199/204)/PAK2 (S192/197) (Cat#2605), p-PAK1 (T423)/PAK2 (T402) (Cat#2601), p70 S6 Kinase (49D7) (Cat#2708), Mouse Anti-rabbit IgG (Conformation Specific) (L27A9) mAb (HRP Conjugate)

(Cat#5127) from Cell Signaling Technology. Goat anti-rabbit IgG-HRP (sc-2054), Goat anti-mouse IgG-HRP (sc-2055), Sur-8 (D-8) (sc-514779), Tiam1 (C-16) (sc-872) from Santa Cruz; HA Tag (A190-208A) from Bethyl, FLAG M2 antibody (F1804) from Sigma-Aldrich; Total OXPHOS human WB Antibody Cocktail (ab110411), UFM1 [EPR4264(2)] (ab109305), p-PAK2 (S20) [EPR658(2)] (ab76419) from Abcam; Raptor (09-217) from EMD Millipore,; and GAPDH (GT239) from GeneTex.

The following antibodies were used for immunofluorescence: UFSP2 (G-11) and GRP94 (C-19) from Santa Cruz; COX IV (3E11), HA-Tag (6E2), FLAG-Tag (D6W5B) from CST; FLAG-Tag (M2) from Sigma; and Donkey anti-Goat IgG (H+L) Secondary Antibody Alexa Fluor 488 conjugate, Donkey anti-Mouse IgG (H+L) Secondary Antibody Alexa Fluor 488 conjugate, Donkey anti-Mouse IgG Secondary Antibody Alexa Fluor 568 conjugate, Donkey anti-Rabbit IgG (H+L) Secondary Antibody Alexa Fluor 568 conjugate, Donkey anti-Mouse IgG (H+L) Secondary Antibody Alexa Fluor 647 conjugate from Thermo Fisher.

Cell Lysis and Immunoblotting
Cells were rinsed twice with ice-cold PBS and lysed with Triton lysis buffer (1% Triton X-100, 20 mM Tris-HCl [pH 7.4], 150 mM NaCl, 1 mM EDTA, 1 PhosSTOP Phosphatase Inhibitor Cocktail tablet per 25 mL buffer [Roche], 1 cOmplete, EDTA-free Protease Inhibitor Cocktail Tablet per 25 mL buffer [Roche]). The cell lysates were cleared by centrifugation at 13,000 rpm at 4°C in a microcentrifuge for 10 min and quantified for protein amount using BCA reagent (Thermo Scientific). Protein samples were normalized for protein content, denatured by the addition of Laemmli buffer and boiling for 5 min, resolved by SDS-PAGE, and transferred to a polyvinylidene difluoride membrane (Millipore). Immunoblots were processed and analyzed according to standard procedures and analyzed using chemiluminescence.

Immunoprecipitation Studies
5 million HEK293T cells stably expressing FLAG-tagged cDNAs were plated in 10 cm culture dishes. For co-immunoprecipitation (co-IP) studies, cells were transfected with 3 μg of the indicated plasmids using XTremeGene 9 Transfection Reagent (Roche) 24 hr after seeding and the cell culture media was changed the following day. 72 hr after seeding, cell lysates were prepared as described above. The FLAG-M2 affinity gel (Sigma) was washed three times with lysis buffer. 40 μl of a 50/50 slurry of the FLAG-M2 affinity gel was then added to clarified cell lysates and incubated with rotation for 90 min at 4°C. Following IP, the beads were washed three times with lysis buffer. For co-IP experiments, immunoprecipitated proteins were denatured by the addition of 40 μl of Laemmli buffer and boiling for 5 min and resolved by SDS-PAGE. For FLAG-C17orf89 mass spectrometry experiments, immunoprecipitated proteins were eluted using the FLAG peptide, resolved rom the FLAG-M2 affinity gel, resolved on 4%–12% NuPage gels (Invitrogen), and stained with simply blue stain (Invitrogen). Each gel lane was sliced into 10-12 pieces and the proteins in each gel slice were digested overnight with trypsin. The resulting digests were analyzed by mass spectrometry.

Immunofluorescence
100 thousand HEK293T cells were seeded on 35 mm fibronectin-coated glass-bottom dishes (MatTek). 24 hr later, cells were rinsed with PBS, fixed with 4% paraformaldehyde in PBS for 15 min, rinsed with PBS again, permeabilized with 0.4% Triton X-100 in PBS for 12 min, rinsed with PBS again, and blocked with 10% horse serum (HS) for 20 min. Dishes were then incubated with primary antibody in 10% HS for 1 hr at RT, rinsed three times with PBS, and incubated with a fluorescent secondary antibody diluted 1:400 in 10% HS for 2 hr at RT in the dark. Finally, cells were rinsed three times with PBS and on the second wash were incubated with DAPI for 20 min. Dishes were imaged on an Axio Observer.Z1 inverted epifluorescence microscope (Zeiss).

Seahorse Analysis
Oxygen consumption of intact cells was measured using an XF24 Extracellular Flux Analyzer (Seahorse Bioscience). XF24 Cell Culture Microplates (Seahorse Bioscience) were coated with Cell-Tak Cell and Tissue Adhesive (Corning), and seeded with 180 thousand Nomo-1 cells (100 μl) per well. The plates were centrifuged to let cells adhere to the bottom, placed in an incubator not supplemented with CO_2 for 30 min, and subsequently analyzed on the XF24 Analyzer.

siRNA Experiments
Nucleofection of siRNAs was performed using the Cell Line Nucleofector Kit V on a Nucleofector Device (Lonza) according to the manufacturer's instructions. Briefly, 5 million SKM-1 cells were pelleted and resuspended in 100 μL Nucleofector solution and 2 μL of either the ON-TARGETplus PREX1 siRNA SMARTpool or the siGENOME Non-Targeting siRNA Pool #1 (100 μM) and transfected using the V-001 program. Cells were then resuspended in pre-warmed IMDM supplemented with 10% IFS to allow for recovery and the same transfection procedure was repeated 24 hr later. 96 hr after the initial transfection, cells were lysed and processed for either immunoblotting as described above or with the Active Rac1 Detection Kit (Cell Signaling Technology) according to the manufacturer's instructions to determine the cellular levels of active, GTP-bound Rac1.

RNA Sequencing
Transcriptomic analysis of PL-21 and OCI-AML2 cells was performed using a strand-specific RNA sequencing protocol described previously. Briefly, total RNA was extracted using the RNeasy Mini kit (QIAGEN). 5 μg of polyA-selected RNA was fragmented and dephosphorylated after which an ssRNA adaptor was then ligated. Reverse transcription (RT) was performed using a primer

complementary to the RNA adaptor after which a DNA adaptor was ligated onto the 3′ end of the resulting cDNA product. The library was then PCR amplified, cleaned, quantified using a TapeStation (Agilent) and sequenced on a HiSeq 2500 (Illumina). Result reads were then mapped to the reference human genome (hg19) using TopHat.

Short-Term Proliferation Assays

ATP-based measurements of cellular viability were performed by plating cells in 200 μL of media in 96-well plates. The number of cells and biological replicates seeded varied depending on the cell line and the duration of the experiment. At the indicated times, 40 μL of CellTiter-Glo reagent (Promega) was added to each well, mixed for 5 min, after which the luminescence was measured on the SpectraMax M5 Luminometer (Molecular Devices). For the drug treatment experiments, FRAX-597, Ruxolitinib, and Selumetinib were obtained from Selleckchem and Quizartinib from LC Laboratories.

Sanger Sequencing

For a subset of the mutant Ras cell lines used in our study, *KRAS* and *NRAS* were subjected to sequencing analysis. Briefly, genomic DNA was extracted and amplified via PCR (primer sequences listed below) to interrogate hotspots in both genes. The PCR products were then purified and sequenced using the Sanger method.

For residues G12, G13, and A18:

KRAS1 forward:	AGGCCTGCTGAAAATGACTGAA
KRAS1 reverse:	AAAGAATGGTCCTGCACCAG
For residue Q61:	
KRAS2 forward:	CTCAGGATTCCTACAGGAAGCA
KRAS2 reverse:	CACCTATAATGGTGAATATCTTCAAAT
For residues K117 and A146:	
KRAS3 forward:	GGACTCTGAAGATGTACCTATGG
KRAS3 reverse:	TCAGTGTTACTTACCTGTCTTGT
For residues G12 and G13:	
NRAS1 forward:	ACAGGTTCTTGCTGGTGTGA
NRAS1 reverse:	CACTGGGCCTCACCTCTATG
For residue Q61:	
NRAS2 forward:	GTGGTTATAGATGGTGAAACCTGT
NRAS2 reverse:	TGGCAAATACACAGAGGAAGC

QUANTIFICATION AND STATISTICAL ANALYSIS

Genome-wide CRISPR Screening

Sequencing reads were aligned to the sgRNA library and the abundance of each sgRNA was calculated. A small number of sgRNAs in both the human and mouse libraries have identical target sequences because they target multiple members of the same highly redundant gene family. Reads mapping to these sequences are assigned to all matching sgRNAs. As the human sgRNA library is comprised of three separate DNA plasmid sub-pools (due to limitations of microarray-based sgRNA synthesis), the counts of the sgRNA within each sub-pool are quantile normalized against each other for each of the initial and final AML samples. The sgRNA counts from all of the initial cell populations of the AML lines and of the two replicate initial Ba/F3 cell populations were combined to generate the human and mouse initial reference datasets, respectively. For each initial reference dataset, sgRNAs with less than 50 counts were removed from downstream analyses. The log$_2$ fold-change in abundance of each sgRNA was calculated for final population samples for each of the cell lines after adding a count of one as a pseudocount. Gene-based CRISPR scores (CS) were defined as the average log$_2$ fold-change in the abundance of all sgRNAs targeting a given gene between the initial and final cell populations and calculated for all screens. The CS reported for the NB4 cell line and the isogenic Ba/F3 experiments was the average of two independent replicate experiments.

Secondary CRISPR Screening

CRISPR gene scores were calculated as with the genome-wide screens with slight modifications. sgRNAs with less than 10,00 counts in the initial dataset were removed from the downstream analysis and a pseudocount of 10 was added prior to the log$_2$ fold-change calculation. Lastly, CRISPR scores were quantile normalized across of all the cell lines screened.

Comparative Essentiality Testing

To compare human gene essentiality with yeast gene essentiality 1-to-1 human-yeast homologs mappings were obtained from the Ensembl Gene release 79 database. Human genes common to the selected genome-wide CRISPR screen datasets were used for comparison. Each dataset was ranked by their respective scores and used to predict the essentiality of yeast homologs (Giaever et al., 2002). The sensitivity and specificity of these predictions were analyzed using receiver operator characteristic (ROC) curves and the area under the ROC curve was used as the performance metric.

Copy Number Peak Analysis

The sliding window score (SWS) for a given gene in a given cell line was defined as the number of nearby genes with a CS in the lowest 3% of all genes in that cell line. For each gene, a window of the 20 nearest 'upstream' and 20 nearest 'downstream' flanking genes was chosen for analysis. As some genomic regions contain many bona fide essential genes (e.g., histone gene clusters), genes essential in all lines were removed prior to the SWS calculation. For this purpose, the average CS of each gene across all cell lines was calculated and genes in the lowest 15% were removed. For each of the remaining genes, the SWS was calculated in each cell line. Genes with SWS > 12 were designated as high SWS genes and removed from the correlated gene essentiality analysis.

Correlated Gene Essentiality Analysis

To maximize the likelihood of identifying biologically meaningful relationship between genes, (1) genes essential in most of the cell lines, (2) genes only essential in a single line or which display erythroid-specific essentiality and (3) genes with low variability in CS across the 14 cell lines were removed from the analysis. For (1), genes for which the second lowest CS was less than −1 were removed. For (2), to assess if a gene was selectively essential in any single cell line, pairwise Pearson's correlation coefficients were calculated between the CS profile of each gene across the 14 cell lines and a 14x14 identity matrix. To assess if a gene was selectively essential in the two erythroid lines, a Pearson's correlation coefficient was calculated between the CS profile of each gene and a vector containing 14 binary variables in which the two variables corresponding to the erythroid lines are set to '1' with the remaining set to '0'. If the maximum absolute value of any of these coefficients was greater than 0.8, the gene was removed. For (3), the variance of the CS profile each gene across the 14 cell lines was obtained. The top 2,000 genes showing the highest variance were included in the correlated essentiality analysis. Select sets of genes with high correlation were highlighted and/or chosen for follow-up validation.

DATA AND SOFTWARE AVAILABILITY

Data Resources

Data resources can be found in Tables S3, S5, and S8. Additional sgRNA-level data and custom scripts for analysis of genome-wide screens are available at: http://sabatinilab.wi.mit.edu/wang/2017/.
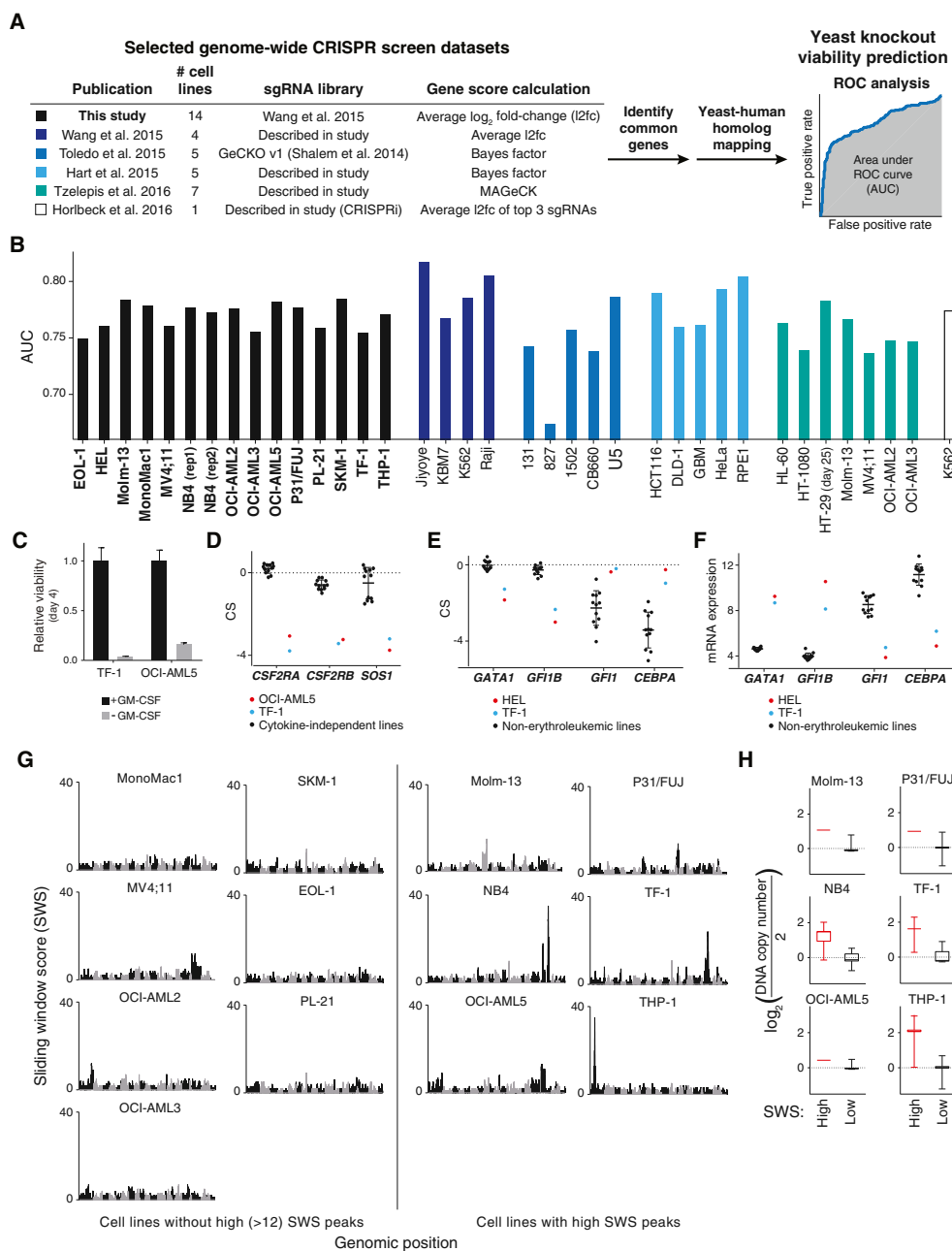
Figure S1. Screen Performance and Sliding Window Score Analysis, Related to Figure 1

(A) Schematic for *S. cerevisiae* homolog essentiality prediction analysis. ROC, receiver operating characteristic.

(B) Performance of selected genome-wide CRISPR screening datasets as assessed by area under the ROC curve.

(C) TF-1 and OCI-AML5 cells require GM-CSF for optimal proliferation. Error bars represent SD from 9 replicate wells.

(D) Genes encoding the heterodimeric GM-CSF receptor, *CSF2RA* and *CSF2RB*, and effector, *SOS1*, scored as the top three most differentially essential genes between the cytokine-dependent and -independent cell lines.

(E) HEL and TF-1 are erythroleukemias whereas the others lines originated from cells of the granulocyte-monocyte (GM) lineage. The erythroleukemic lines selectively require erythroid transcription factors (TFs) *GATA1* and *GFI1B*, whereas the GM-lineage-derived lines selectively require GM lineage TFs, *GFI1* and *CEBPA*.

(F) The TFs identified in (E) also have lineage-selective mRNA expression patterns.

(G) SWS analysis of the other 13 AML cell lines, as performed for HEL in Figure 1D, reveals 6 additional lines with high SWS (> 12) genes.

(H) DNA copy number analysis of high and low SWS genes.

A

Related to Figure 2C

Correlation with *MAPKAP1*

MLST8	0.96
RICTOR	0.82

Correlation with *NPRL2*

NPRL3	0.91
DEPDC5	0.89

Related to Figure 2D

Correlation with *FANCF*

FANCC	0.90
C17orf70	0.90
FANCA	0.89
BRIP1	0.86
FANCG	0.85
FANCI	0.84
FANCL	0.84
UBE2T	0.84
FANCE	0.82

Related to Figure 2F

Correlation with *TP53*

MDM4	0.87
MDM2	0.88
TERF1	0.74
PPM1D	0.73

Related to Figure 2G

Correlation with *FURIN*

IRS2	0.88
IGF1R	0.88

Correlation with *DDI2*

NGLY1	0.89
NFE2L1	0.87

Related to Figure 3A

Correlation with *C1orf27*

UFSP2	0.87
UFC1	0.82
UBA5	0.79
UFL1	0.65
UFM1	0.57

Related to Figure 3G

Correlation with *C17orf89*

PDE12	0.87
NDUFAF5	0.85
NDUFS5	0.84
COQ7	0.83
NDUFAF7	0.83
NDUFC2	0.82
TIMMDC1	0.82
NDUFA6	0.81
ACAD9	0.8
NDUFA2	0.8
NUBPL	0.78
NDUFS2	0.76
CPOX	0.76
NDUFA9	0.75
MTO1	0.74
NDUFAF4	0.74
YBEY	0.74
NDUFAF1	0.73
NDUFV1	0.73
NDUFAF3	0.72

Related to Figure S2B

Correlation with *SOS1*

GAB3	0.90
PTPN11	0.88
JAK2	0.83
CSF2RA	0.83
CSF2RB	0.82
GRB2	0.80

B

GM-CSF receptor signaling pathway

cytokine status:
○ dependent
● independent

● GAB3
● PTPN11
● JAK2
● CSF2RA
● CSF2RB
● GRB2

SOS1 CS

C

Gene	wild-type *TP53* lines (avg. CS)	mutant *TP53* lines (avg. CS)	t-test of differential essentiality (p-value)
TP53	1.62	-0.39	4.8×10^{-5}
MDM4	-1.82	0.08	2.6×10^{-5}
MDM2	-2.45	-0.1	2.9×10^{-7}
TERF1	-2.11	-0.79	7.1×10^{-4}
PPM1D	-2.48	-0.9	5.3×10^{-4}

Figure S2. Additional Co-essentiality Analysis, Related to Figure 2

(A) Correlation coefficients (Pearson's *r*) for co-essential multi-gene clusters.

(B) Members of the GM-CSF receptor signaling pathway display correlated essentiality. Open circles denote CS of the two GM-CSF-dependent cell lines.

(C) Welch's two-sided t test was applied to assess differential gene essentiality of *TP53* co-essential genes between wild-type and mutant *TP53* cell lines.
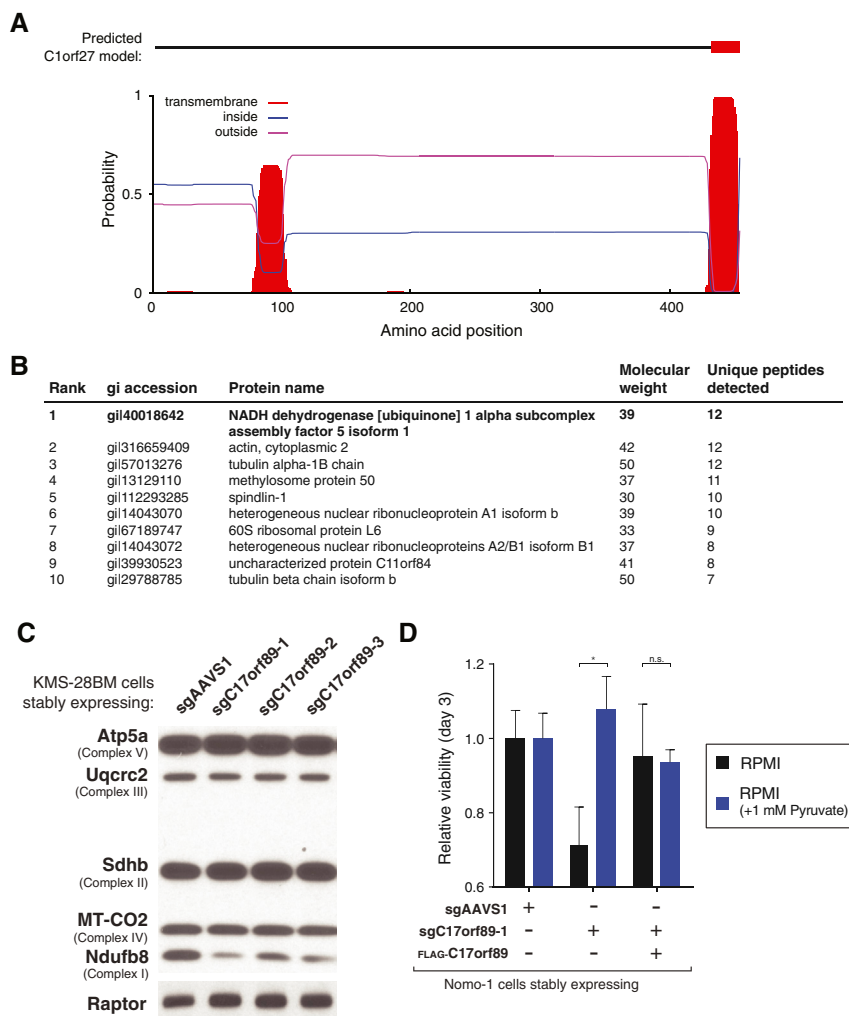
A

Predicted
C1orf27 model:

(plot: Probability vs Amino acid position; legend: transmembrane, inside, outside)

B

Rank	gi accession	Protein name	Molecular weight	Unique peptides detected
1	gi|40018642	**NADH dehydrogenase [ubiquinone] 1 alpha subcomplex assembly factor 5 isoform 1**	**39**	**12**
2	gi|316659409	actin, cytoplasmic 2	42	12
3	gi|57013276	tubulin alpha-1B chain	50	12
4	gi|13129110	methylosome protein 50	37	11
5	gi|112293285	spindlin-1	30	10
6	gi|14043070	heterogeneous nuclear ribonucleoprotein A1 isoform b	39	10
7	gi|67189747	60S ribosomal protein L6	33	9
8	gi|14043072	heterogeneous nuclear ribonucleoproteins A2/B1 isoform B1	37	8
9	gi|39930523	uncharacterized protein C11orf84	41	8
10	gi|29788785	tubulin beta chain isoform b	50	7

C

KMS-28BM cells stably expressing: sgAAVS1, sgC17orf89-1, sgC17orf89-2, sgC17orf89-3

Atp5a (Complex V)
Uqcrc2 (Complex III)
Sdhb (Complex II)
MT-CO2 (Complex IV)
Ndufb8 (Complex I)
Raptor

D

(bar graph: Relative viability (day 3); legend: RPMI (black), RPMI (+1 mM Pyruvate) (blue))

sgAAVS1	+	−	−
sgC17orf89-1	−	+	+
FLAG-C17orf89	−	−	+

Nomo-1 cells stably expressing

Figure S3. C1orf27 and C17orf89 Characterization, Related to Figure 3

(A) Transmembrane domain prediction analysis for C1orf27 using the Transmembrane Helices Hidden Markov Models tool version 2.0.

(B) Mass spectrometry analysis of anti-FLAG immunoprecipitates prepared from HEK-239T cells stably expressing FLAG-C17orf89.

(C) C17orf89 loss results in the selective destabilization of mitochondrial complex I in KMS-28BM cells.

(D) C17orf89 loss results in a selective reduction in the proliferation of Nomo-1 cells cultured in the absence of pyruvate. This phenotype was rescued by the expression of an sgRNA-resistant C17orf89 cDNA. Error bars represent SD from 4 replicate wells. * denotes p < 0.05, Welch's two-sided t test.
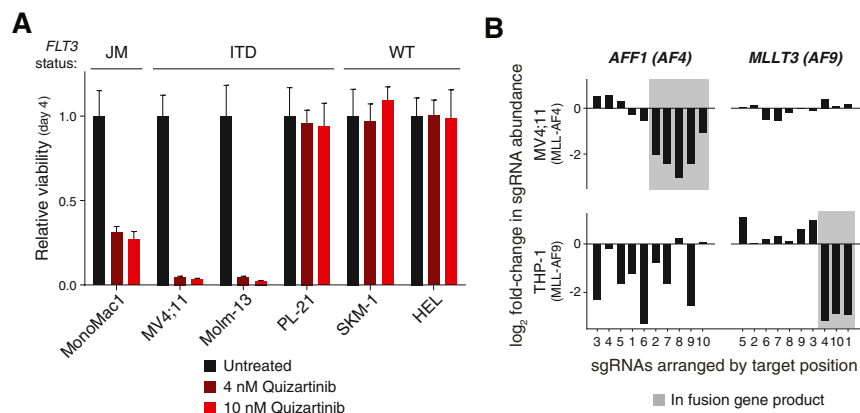
Figure S4. Validation of *FLT3* Dependence and Analysis of *KMT2A* (MLL) Fusion Oncogenes, Related to Figure 4

(A) Treatment with a small-molecule inhibitor of FLT3, quizartinib, recapitulates essentiality data obtained from genome-wide CRISPR screens. Error bars represent SD from 5 replicate wells. JM, juxtamembrane domain mutation (presumed to be activating). ITD, internal tandem duplication.

(B) sgRNA-level analysis of two MLL translocation partners. MV4;11 and THP-1 cells carry the *MLL-AF4* and *MLL-AF9* fusion oncogenes, respectively, and display selective depletion of sgRNAs targeting regions that encode the fusion gene products.
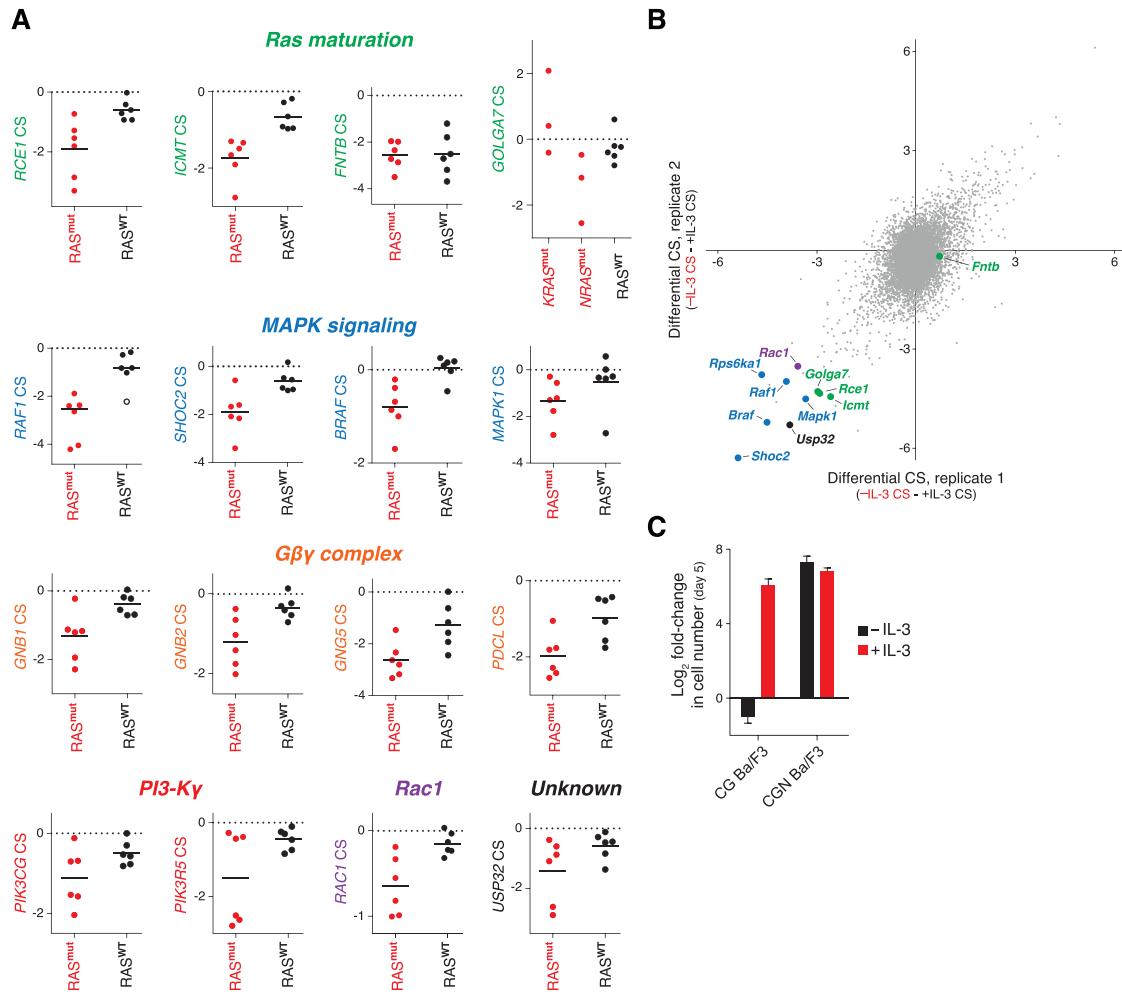
Figure S5. Additional Ras Synthetic Lethal Candidates, Related to Figure 5

(A and B) Additional gene candidates displaying synthetic lethality with oncogenic Ras identified from screens in (A) human AML and (B) murine CGN Ba/F3 cells.

(C) Proliferation of CG and CGN Ba/F3 cells cultured in the presence or absence of 1 ng/uL IL-3. Error bars represent SD from 10 replicate wells.
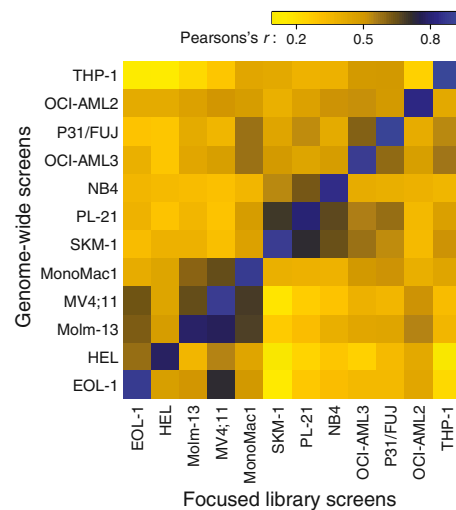
Figure S6. Genome-wide and Focused sgRNA Library Screens Show High Concordance, Related to Figure 6

All 12 cytokine-independent AML cell lines screened using the genome-wide sgRNA library showed the highest correlation with focused sgRNA library screens conducted in the same line.